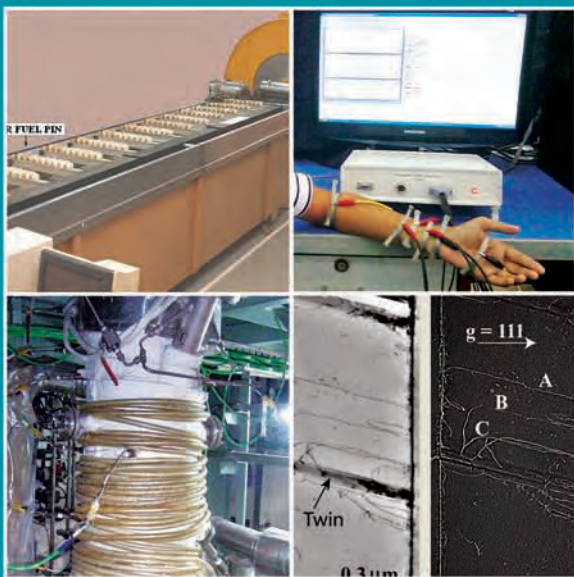# BARC
NEWSLETTER

IN THIS ISSUE

- Studies on Improvements in Thoria Dissolution Process for Reprocessing Application

- Characterization of Deformation Microstructure using Transmission Electron Microscopy

- Early Detection of Coronary Heart Disease using Peripheral Pulse Analyzer

- Development of Fluidized Bed Thermal Denitration

- MetProSoft-10: Image Analysis Software for Metallographic Measurements

- Passive Gamma Scanning – A Powerful Tool for QC of MOX Fuels

In the Forthcoming Issue

CONTENTS

From the Editor's Desk

Shri Sekhar Basu took over as Director, BARC in June 2012. Through the forum of the BARC Newsletter, he addresses the BARC fraternity for the first time in this issue.

We have received encouraging response for our new feature "Brief Communication" introduced from this year. Several readers have appreciated our efforts. Kindly contribute your recent and important accomplishments for this feature.

This issue carries six interesting articles on various R&D areas of BARC. Thoria dissolution a matter of importance was discussed and one of the articles presents details of this process and its beneficial impact on the downstream HLW vitrification process. The application of transmission electron microscopy technique for characterizing dislocations, defect and deformation microstructure has been well discussed with special reference to gamma-TiAl alloys in another article.

I do hope that these articles will provide information to Scientists working in these areas and also to others working in overlapping areas.
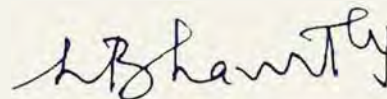
Dr. K. Bhanumurthy
On behalf of the Editorial Committeee

Message From the Desk of the New Director of BARC

It gives me great pleasure in addressing you all through the forum of BARC Newsletter. On my assuming the new role and responsibility as the eleventh Director of this prestigious research centre, BARC, I feel much honoured to lead this institution that was steered earlier by several towering stalwarts. I will do my best to uphold the highest tradition set by my predecessors in terms of excellence and relevance in all aspects of Nuclear Science and Technology programmes and projects. I look forward to the support and cooperation from the entire fraternity of DAE in general, and BARC in particular, to fulfil the onerous commitments that I have taken up on becoming the Director of BARC.

I am fortunate to have been associated with the entire backend of the nuclear fuel cycle programme in the recent past. This area holds the key to bridging the first and second stage of the Indian Nuclear Power Programme (INPP). In this regard, there is excellent performance of the new recycle plants at Tarapur and Kalpakkam, and also satisfactory progress on the integrated fuel reprocessing facility, which is also coming up at Tarapur. It is important to continue to maintain our momentum in this direction, as we get involved in commissioning more indigenous nuclear reactors (PHWRs) and also plan for processing the spent fuel in the safeguarded domain.

Research and Development related to advanced nuclear reactors and energy systems, taken along with the associated fuel cycle aspects, is at the core of BARC activities. Apsara, our oldest research reactor, will be refurbished with a new core and we are planning to build two more high flux research reactors. In connection with the utilisation of thorium, our focus will continue to be on the Advanced Heavy Water Reactor (AHWR), apart from working further on the engineering aspects of the Compact High Temperature Reactor (CHTR) and also addressing development of certain enabling technologies required for the ADS programme. BARC will collaborate with NPCIL in designing and developing the Indian light water reactors (IPWR) in addition to providing need-based R&D support to the operational PHWRs. Nurturing advanced R&D in both basic sciences and engineering topics, while keeping a focus on directed research wherever possible, will continue to remain the time-tested BARC tradition.

Societal benefits of nuclear applications are immensely important for the very large population of our nation. BARC has a strong base and well-established role in contributing to agricultural productivity, healthcare management, enhancing water quality and availability, food preservation and safety and effective management of several industrial processes, as well as development of advanced materials and sophisticated instruments/systems. Many of these are achieved through either the application of radioisotopes and radiation technologies or as spin-off from our pursuit of various indigenous technology developments related to mainstream nuclear programmes. BARC will continue to further develop similar relevant

technologies and their applications and also transfer the appropriate ones for commercial exploitation. I look forward to fostering a multi-fold increase in all the activities bringing direct societal benefits.

There is an increasing global interest in seeking Indian contributions to major international projects such as the ones related to building large accelerators. At the same time, the India-based Neutrino Observatory (INO) is a multi-institutional major initiative aimed at building a world-class underground laboratory for non-accelerator based high energy and nuclear physics research in India. While BARC may not be the host organisation in these cases, BARC will play every possible role to support such mega-science projects.

Harnessing the synergies of various disciplines as well as of the multiple competencies of the talented human resources of BARC is essential for achieving all our above goals and targets. I strongly urge for nurturing team building in all our activities, so that we work together as effective members of a single large professional community to fulfil the aims and objectives of our organisation as well as ensure timely deliverables to DAE and/or our society at large.

The BARC Newsletter has been an important medium to showcase our progress and achievements and its Editorial Committee is doing a commendable job in highlighting recent developments and other relevant R&D activities. The BARC Newsletter enjoys a wide readership both among BARC fraternity as well as outside BARC. The new feature "Brief Communications" introduced this year has added to its range of content and quality. I wish the BARC Newsletter many more successes and new features to reach out to a still larger readership in the coming years.
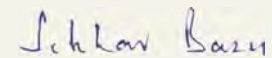
Sekhar Basu
Director, BARC

H$_2$-F$_2$ Flame Reactor Technology for Nuclear Material Processing

Chemical Technology Group

Many chemical processes of industrial importance require higher temperatures which can be facilitated by in-situ generation of heat through an exothermic chemical reaction in a flame reactor. These reactors offer wide range of applicability from nano-particle synthesis to nuclear processing. An experimental facility comprising of the fluorine generation system, the H$_2$-F$_2$ flame reactor, the feeding system and the scrubbing system has been set up and commissioned in Chemical Technology Division of BARC. The gases handled are toxic and potentially explosive. Methodologies have been devised and necessary arrangements are made to ensure safe and controlled operation. The process parameters can be tuned according to the reactor temperature requirement. This technology is predominantly advantageous as a flame heat source for those chemical processes where oxide contamination of the final product is not desirable.

The facility is being routinely used for the chemical processing in which the produced material is useful for the front end of the nuclear fuel cycle. The new flame reactor technology has been able to (a) reduce the number of processing steps, equipments and the effluent generation and, (b) yield product of desired quality.

The deployment of the flame reactor technology can be further extended to develop the novel processes in the back end of nuclear fuel cycle.

The flame reactor facility

The fluorine cell

The end product from flame reactor technology (Final processing done at UED, BARC)

Force Reflecting Telerobot

Design Manufacturing & Automation Group

The Force Reflecting Telerobot is a recent development in remote handling manipulation and is an upgraded version of the Advanced Servo Manipulator developed by Divn. of Remote Handling & Robotics. It consists of two identical articulated arms, the master arm and the slave arm, connected electrically. The slave arm is usually kept in remote hazardous environment and the master arm in a safe operating area. In addition to master following mode, the slave arm can also be controlled as a robot through a computer. The force reflecting telerobot represents a new generation of remote handling technology with advanced features like position control of the slave arm in world coordinates, indexing in world coordinates, scaling of slave motion, constrained motion, teach & playback and interactive robot control etc. This development involves many challenging tasks in electrical, electronics, control and software areas.

The telerobot is provided with six Degrees of Freedom and has a payload of 25 kg. It has a maximum reach of 1.2 m and the gripper opening is 100 mm. The force reflection ratio varies from 0 to 1 and the maximum force reflected is 8 kg.

The joints of the arms are actuated by Permanent Magnet Synchronous servo motor with built-in resolver & fail-safe brake. Ethernet based servo drives have been developed for the control of these motors. The controller provides variable force reflection, controllable slave capacity; user defined slave workspace, artificial force reflection and programmed motions to follow a sequence of configurations. Indexing is provided so that the slave joints can be rotated without moving the master. The telerobot can have elbow-up or elbow-down configuration for ease of operation.

The slave arm can handle heavy objects with less operator's effort. The slave arm can be mounted on a transporter to augment its operating range; hence, hot cell size is independent of manipulator reach. Telerobot provides flexibility in designing and laying out hot cell equipment since the slave arm can approach equipment from multiple directions in the hot cell. Expensive radiation shielding window can be avoided by using CCTV cameras. Telerobot is suitable for repeatable task in hot cell.

Force Reflecting Telerobot

Development of Plate Thermometer (PT) for Heat Flux Measurement

Reactor Design & Development Group

Application:

For Heat Flux Measurement during Thermal Qualification (Open Pool Fire/ Furnace tests at 800 Deg.C for 30 mins) specified by AERB/IAEA Transport Regulations for Type-B radioactive material transportation packages.

Advantages over Conventional devices like Schmidt Boelter/ Gardon Gauges:

• Economical (Rs.2000 for PT Vs Rs.3 Lakh for Water Cooled) and hence requisite numbers (60-70 Nos for each Pool Fire Experiment) can be deployed

• Easy to Construct, Operate and Calibrate

• Does not need Cumbersome Water Cooling through Extremely Hot Zones of Pool Fire.

• Only Single Temperature Measurement of PT Vs Two Temperature Measurements in addition to one Water Flow Measurement of Conventional gauges

History and Development of Plate Thermometers

• Developed by Wickstrom, in 1980s, for controlling fire resistance furnaces to get harmonized test results.

• Demonstrated by Ingason and Wickstrom, in 2006, for measuring the incident radiant heat flux as an alternative to water cooled heat flux sensors.

Re-engineered and calibrated in the laboratory of IIT- Bombay for large scale deployment in pool fire and furnace tests conducted for package qualification.

Plate Thermometer with Insulation Back Pad

Construction of Plate Thermometer

• Thin steel plate of dimensions: 100 mm × 100 mm and 0.7 mm thick

• Coating and Curing of a Paint with High and Known Absorptivity at Measuring side

• An insulating fiber board on one side

• A thermocouple welded to the center of the plate.

Activities conducted during adoption of Plate Thermometer:

• Selection of plate material, backing insulation, the coating used for controlling the surface absorptivity of plate and the thermocouple, as consistency of Heat Flux measurement completely depends upon their thermal characteristics

• Standardization of Coating-Curing methods of High Absorptivity Paint in the temperature range of $30^{o}C$ to $1200^{o}C$, expected during pool fire/furnace tests

• Calibration using Cone Calorimeter to correlate the temperature readings to heat flux values

• Analytical Modeling and Simulation of PT performance for measuring incident radiative heat flux considering the thermal properties of materials, geometry, heat transfer, heat balance and losses including convection that occur during its operation.
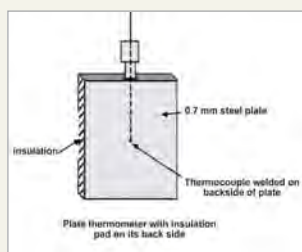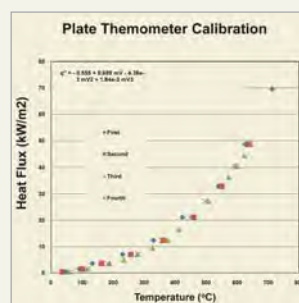
Importance of curing method:

Plate with Coating (a) Before Curing (b) After Curing

Calibration of Plate Thermometer (PT) in Cone Calorimeter

Development of Metal – Ceramic Seals for Neutron Detectors

Materials Group

Neutron detectors are used in Na-cooled fast breeder reactors for monitoring the neutronics at various locations. These detectors require vacuum tight metal–ceramic feedthroughs, having leak rate less than 5×10^{-9} mbar/l. Since the life of these detectors is very long, the metal–ceramic joints need to perform continuously at high temperatures of about 500-550 °C without degradation. In the present design, a suitable methodology for bonding alumina tubes to Inconel 600 ferrules of the feed-throughs, with such stringent specifications, was developed.

Leak-tight alumina–Inconel 600 joints were produced using two different brazing routes. In one of the methods, Au-18 wt.% Ni alloy foil was used to braze pre-metallized alumina tubes with Inconel 600 ferrules, while in the other, active metal brazing route was adopted, in which Silver-ABA alloy foils was used for brazing the two components directly. The joints prepared by both these methods showed leak rates better than 5×10^{-10} mbar-l/sec, in as-joined condition. Both types of joints were subjected to simulated in-service conditions and were exposed to high temperatures in the range 400-600 °C for prolonged time, under flowing argon for duration ranging up to 480 days. The joints prepared by both the methods met all the stringent specifications.

Extensive microstructural and microchemical characterisation of these joints showed absence of pores, voids or micro-cracks at the metal-ceramic interfaces. Mechanical testing revealed that the stress-to-failure of these joints were adequate for these applications. In all cases, the failure occurred on the alumina side of the joint, therefore indicating that the strength of the metal-ceramic interfaces is higher than that of alumina. The residual stresses produced in the joint were estimated using finite element modelling, which showed that the thermal stresses generated due to difference in coefficient of thermal expansion could be well accommodated due to ductile nature of the braze alloy.
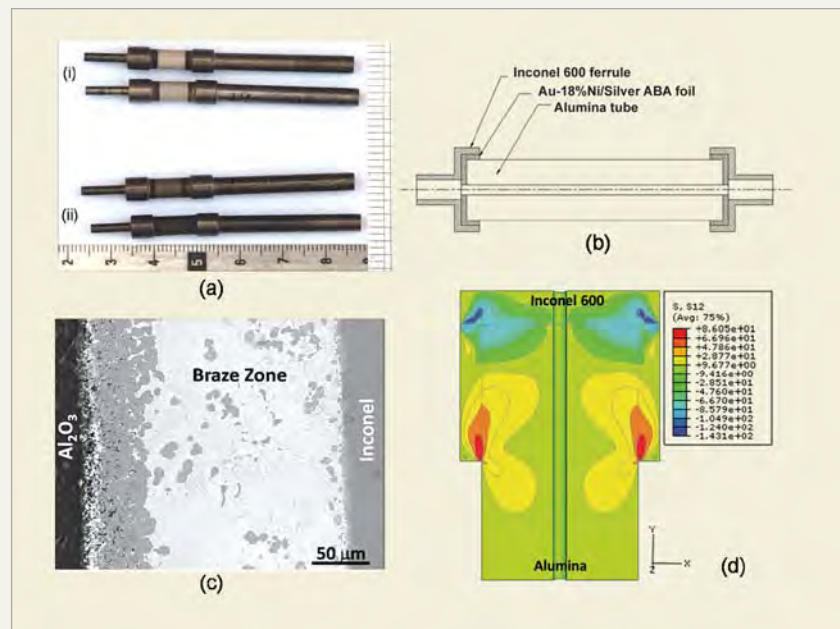

Fig. 1 (a) Alumina-Inconel 600 joints in (i) as-brazed and (ii) annealed conditions, (b) schematic diagram showing arrangement of the joint assembly, (c) microstructure of the cross-section, and (d) distribution of the residual shear stress t_{12}.

Studies on Improvements in Thoria Dissolution Process for Reprocessing Application

C. Srinivas, Vrunda Yalmali, A.S. Pente, P.K. Wattal and S.D. Misra

Nuclear Recycle Group

Abstract

Thoria dissolution is normally conducted in 13M nitric acid in the presence of 0.03M sodium fluoride or HF as catalyst and 0.1M aluminium nitrate for mitigation of fluoride related corrosion of SS 304L dissolver vessel. Addition of aluminium nitrate in such high concentrations has undesirable consequences in the downstream high level radioactive liquid waste vitrification process. Besides, because of the highly corrosive nature of fluoride ion, lowering its concentration in the dissolution reaction is advantageous in reducing the corrosion of dissolver and other downstream equipments. The present work was done with twin objectives of avoiding aluminium nitrate addition and lowering the fluoride ion concentration during dissolution reaction. High temperature sintered thoria pellet dissolution reactions were investigated in the absence of aluminium nitrate and at reduced fluoride concentrations. Corrosion rates of SS 304L and zircaloy in various dissolvent mixtures were studied by weight loss method. These studies clearly showed that aluminium nitrate addition for control of fluoride related corrosion of SS 304L can be avoided when zircaloy-clad thoria pellets are dissolved. Moreover, dissolution could be achieved with reasonable reaction rates at reduced fluoride concentration of 0.005-0.01M instead of 0.03M by changing the method of addition of the fluoride catalyst.

Introduction

In Thoria dissolution process, presence of aluminium ion at high concentrations (0.1M) for mitigation of fluoride effected corrosion of SS 304L dissolver leads to undesirable consequences in the downstream vitrification process adopted for management of high level radioactive waste. These include reduction in waste loading, foaming and high viscosity of the glass melt. Therefore, it is advantageous to avoid or minimize the use of aluminium ion during thoria dissolution.

It is known that fluoride ion forms strong complexes not only with aluminium but also with zirconium, thorium ions etc. The stability of the 1:1 complexes in decreasing order is as follows [1, 2]:

$$Zr(IV) > Th(IV) > Al(III) > Be(II) > Fe(III)$$

Zircaloy will be used as a clad material for power reactor thoria based nuclear fuels. In the presence of fluoride ion, zirconium in the clad material dissolves, to some extent, in the nitric acid medium.

Dissolved zirconium ion can complex with free fluoride more effectively than aluminium ion and inhibit corrosion. Besides, aqueous thorium ions forming from Thoria dissolution reaction can also complex with fluoride ion and inhibit corrosion [2, 3]. It was, therefore, felt that addition of aluminium nitrate may not be required to mitigate the dissolver corrosion. A detailed experimental study was done to verify this assumption. Dissolution reaction was also studied at fluoride concentrations less than the standard 0.03M.

Materials and Methods

High temperature sintered thoria pellets were procured from RMD, BARC and used in the experiments. Zircaloy-2 was procured from MSD and AFD, BARC for the experiments. Other chemicals used were of AR grade and used as received. Sodium fluoride was used as catalyst in all the experiments. Plain, polished SS 304 L coupons having surface area 15-26 cm^2 were used in the experiments for corrosion study by weight loss method.

The study was restricted to dissolution in 13M nitric acid with varying concentrations of sodium fluoride.. The ratio of the volume of 13M nitric acid to the weight of thoria pellet was maintained at nearly 4.0. This will simplify the feed preparation for the subsequent THOREX solvent extraction step without the acid killing step by formaldehyde.

Thoria dissolution reaction is very slow in comparison with that of uranium dioxide. In order to monitor the progress of the thoria dissolution reaction, solution samples were, therefore, drawn conveniently at 24 hour intervals. Thorium content in the sample was estimated titrimetrically with EDTA reagent using xylenol orange indicator. Residual thoria weight was also measured at the end of the experiment after washing and drying.

In order to study the corrosion of SS 304L and zircaloy-2, polished coupon of SS 304L along with

zircaloy-2 tube was placed in the dissolvent mixture during the dissolution experiment. In order to simulate the actual dissolution process conditions more closely, zircaloy tube was used as clad around the oxide pellet in some of the later experiments and effect on dissolution reaction kinetics was studied. Corrosion of SS 304L and zircaloy was studied by weight loss method.

Results & Discussion

Results obtained on thoria dissolution kinetics at different fluoride concentrations and corrosion data were presented in the following sections of the report.

Dissolution studies at 0.03M fluoride concentration

Results of the experiments with standard thoria dissolvent consisting of the formulation, viz., 13M

Table 1: Sintered Thoria pellet dissolution reaction in 13M nitric acid in the presence of 0.03M sodium fluoride and 0.1M aluminium nitrate and zircaloy under boiling and reflux conditions

Run No.	Reaction Time (Hours) For				SS 304L corrosion rate (mpy)	Zirconium concentration in dissolvent (g/l)	Remarks
	80-85% dissolution	85-90% dissolution	90-95% dissolution	95-100% dissolution			
1*	--	--	--	24	44	Not applicable	5 hour sampling showed 53% dissolution and SS corrosion of 161 mpy
2**	-	24	40	72	12	Not applicable	5 hour sampling showed 33% dissolution
3	24	48	--	72	5	1.8	--
4	27	45	--	71	14	1.83	--
5	24	48	--	72	13	4.2	--
6	24	35	53	72	6	4.9	--

*Zircaloy and aluminium nitrate were not added in the reaction mixture;
**Zircaloy was not added in the reaction mixture

nitric acid and 0.03M sodium fluoride in the presence of 0.1M aluminium nitrate and zircaloy were shown in table 1:

In the experimental run no.1 in the table 1, aluminium salt and zircaloy addition was intentionally avoided to see the effect on kinetics and corrosion rate. The reaction progressed rapidly in the absence of zircaloy and aluminium salt and completed in 24 hours. 53% reaction occurred in just 5 hours. In this reaction, the only fluoride complexing metal ion is the reaction product, thorium (IV). This could be the reason for the high initial rate of thoria dissolution. However, it took 24 hours for the completion of the reaction. This could be on account of the increased extent of fluoride complexation by thorium ions. Other factors such as decrease in available thoria pellet surface area, nitric acid concentration and boiling temperature with the progress of the reaction are also responsible for the decrease in the rate of the reaction. The reaction is kinetically controlled with an apparent activation energy of 19 kcal/mole at 0.03M fluoride concentration. The initial dissolution rate expression was reported to be as follows [3]:

$$-\frac{d}{dt}[ThO_2] = k\,[HNO_3]\,[HF]^{0.5}$$

Initial Corrosion rate of SS 304L coupon in the run no. 1 was very high, being 161 mpy in 5h period. This could be attributed to the following factors: Fluoride ion in the reaction mixture can participate in the three following competitive reactions [4,5]:

1) It can get adsorbed on the active sites of thoria surface and form surface complex

2) It can complex with aqueous metal ions such as thorium, zirconium, aluminium. None of these ions are present initially in this experimental run. Equilibrium concentration of fluoride in the solution is expected to change with time and depends on factors such as concentration of each metal ion, concentration of acid, thoria pellet surface area. Therefore, it is a complex system of multiple reactions

3) Fluoride can heterogeneously react with metallic surfaces such as SS and zircaloy resulting in their corrosion. This, in turn, depends on the thermodynamic and kinetic aspects of these reactions.

In run no. 2, 0.1M aluminium nitrate was added to see the change in the kinetics and, especially, the corrosion rate of SS. Corrosion rate reduced from 44 to 12 mpy on account of the complex formation of fluoride with aluminium ion initially and subsequently with thorium ion also. Reaction time has increased by a factor of 3: from 24 in run no. 1 to 72 hours in this experiment. This could be attributed to the presence of two fluoride complexing ions in solution: Al, right from the beginning and Th ions with the progress of reaction. Therefore, in the initial five hour period, the progress was only 33% (ca. 53% in run no.1). In the subsequent runs in table-2, aqueous zirconium ions forming from zircaloy corrosion were also present. Corrosion rate varied from 5-14 mpy in different experiments. Reasons for the variation in the corrosion rates of zircaloy and SS are not entirely clear. However, it could be due to some changes in the surface characteristics of thoria pellets in different experiments which affect the aqueous fluoride adsorption.

In the next series of experiments, thoria dissolution experiments were conducted *in the presence of zircaloy without addition of aluminium nitrate.* Results of these experiments were shown in table-2 below:

Table 2 clearly shows that the absence of aluminium nitrate in the dissolvent did not increase the corrosion rate of SS 304L. Corrosion rate in the present system is in the range of 6.5-11.5 mpy (ca. 5-14 mpy-table1). Therefore, it is clear that zirconium dissolving from zircaloy clad along with thorium ion was able to control the corrosion of SS 304L even in the absence of aluminium salt. *It is significant to note that though the reaction between*

Table 2: Sintered Thoria pellet dissolution reaction in 13M nitric acid in the presence of 0.03M sodium fluoride and zircaloy under boiling and reflux conditions: Al salt concentration: Nil

Run No.	Reaction Time (Hours) For			SS 304L corrosion rate (mpy)	Zirconium concentration in dissolvent(g/l)	Remarks
	85-90% dissolution	90-95% dissolution	95-100% dissolution			
7	24	--	48	6.5	1.3	NaF was added all at once in the beginning of the reaction
8	24	--	47	10	1.4	In the first five hours, NaF was 0.01M; after 5 hours, increased to 0.03M in the solution
9	--	24	47	11.5	1.8	---do---
10	---	48	72	7.7	2.8	Pellet was enclosed in zircaloy tube; split addition of fluoride was used; pellet density:9.43 g/cc; 24 h reaction gave 80-85% dissolution
11	24	48	72	7.8	2.1	--do--; pellet density: 9.38 g/cc

fluoride ion and zircaloy is heterogeneous, in contrast to the homogeneous Al and F ion reaction, it did not lead to excessive corrosion of SS 304L, presumably due to more favourable thermodynamic factors for zircaloy-F⁻ reaction vis a vis SS-F⁻ reaction. Considering this biphasic reaction aspect, fluoride addition into the dissolvent was done in two installments, initially maintained at lower 0.01M and with time gap of 5 hours (referred to as split addition hereinafter) restored to 0.03M in all the experimental runs except the first one of table-2.

Cladding of zircaloy around the pellet, expectedly, resulted in increase of reaction time from 48 to 72 hours. Results presented in table-2 clearly showed that addition of aluminium nitrate is not necessary during zircaloy clad thoria dissolution.

Dissolution studies at 0.01M sodium fluoride concentration

In the following paragraphs, effect of lowering fluoride concentration from 0.03M would be reported.

Table 3: Zircaloy-clad sintered Thoria pellet dissolution in 13M nitric acid in the presence of zircaloy and 0.01M NaF under boiling and reflux conditions

Run no.	Reaction Time (hours) for				SS 304L corrosion rate(mpy)	Zirconium concentration in dissolvent (g/l)	Density of pellet (g/cc)
	70-80% dissolution	80-90% dissolution	90-95% dissolution	95-100% dissolution			
12	24	--	48	72	8.6	0.86	8.65
13	24	48	--	72	8.8	1.02	8.67
14	24	48	72	96	8.4	0.73	9.96

Table 4: Thoria pellet dissolution at 0.005M NaF concentration; Mode of NaF addition: split mode; boiling and reflux conditions

Run no.	Reaction Time (hours) for					SS 304L corrosion rate (mpy)	Zirconium concentration in dissolvent (g/l)
	60-70%	70-80%	80-90%	90-95%	95-100%		
15	48	72	100	--	122	3.5	0.1
16	--	48	--	72	96	6.4	0.31
17	48	--	72	95	115	--	0.4
18	48	--	70	94	123	4.8	0.26
19*	24	48	--	72	120	8.6	0.41

3 hours interval in the split mode of fluoride addition instead of 24 hour in the other runs; zircaloy ring enclosed the pellet; pellet density: 9.9 g/cc

Results of thoria dissolution at 0.01M NaF concentration were shown in table-3. In these experiments, split addition of fluoride was adopted. This was done by maintaining initial fluoride concentration at 0.005M followed by 0.01M after 3h of reaction period. In all these experiments, *the thoria pellet was enclosed in zircaloy clad ring.* At the end of 3h reaction period, 12-14% dissolution occurred in these experiments implying build up of about 0.1M thorium ion concentration in the dissolvent.

Table 3 shows that at 0.01M fluoride concentration also, quantitative dissolution of thoria pellets occurred. SS corrosion was less than 9 mpy, about 10-15% less than the average values (10 mpy) obtained for 0.03M fluoride experiments. *Interestingly, the reaction time was only 72 hours in experiments with low density pellets (run nos. 12&13).* This was the reaction time observed at 0.03M fluoride concentration (table-2). In the experiment with denser pellet in run 14, the reaction time increased to 96 hours with > 90% being complete in 72 h. It appears that by adopting split addition of NaF, zirconium dissolution rate in the reaction mixture can be lowered in the early stages of reaction and faster thoria dissolution rates can

be achieved *without the need for higher fluoride concentration*. The limiting concentration of dissolved zirconium reached about 0.01M in all the experiments which is, incidentally, equal to the fluoride catalyst concentration. Similar observations were reported in the literature [6].

Dissolution studies on thoria at 0.005M fluoride concentration

Table 4 gives the data at 0.005M sodium fluoride concentration for thoria pellets. Corrosion of SS 304L has reduced further at this lower fluoride concentration. It varied from 3.5 to 8.6 mpy It took 72-94 hours to complete 90-95% dissolution in most runs.

Further progress was monotonous and required about 120 hours. Once again, the zirconium concentration during dissolution reaction reached a limiting concentration equal to that of fluoride in the reaction mixture. These results clearly show that NaF concentration as low as 0.005M (1/6th of the presently used value) could also be employed in split mode to achieve >90% dissolution of thoria in 72-96h. Experiments were also conducted on sintered Thoria-4 weight% MOX pellets and the results were similar to those obtained for Thoria

pellets. Detailed report on Thoria and Thoria-Urania dissolution studies is under preparation.

Conclusions

In the present study, thoria dissolution at three different sodium fluoride concentrations, viz., 0.03, 0.01 and 0.005M was investigated. In addition, effect of avoiding aluminium nitrate addition during dissolution reaction was studied on corrosion of SS 304L in the presence of zircaloy clad material. These experimental results clearly showed that when zircaloy clad material is present during dissolution of thoria, addition of aluminium nitrate is not necessary for mitigating corrosion. This would have beneficial impact on downstream HLW vitirification process.

Fluoride concentration can be reduced from the presently adopted 0.03M to lower concentrations by judicious addition of the fluoride catalyst solution. Reaction times for dissolution reaction were observed to be 48-72, 72-96 and 96-120 hours for 0.03, 0.01 and 0.005M respectively depending on density of the sintered pellets used. The reaction times are expected to decrease further in the dissolution of irradiated Thoria pellets.

Acknowledgements

References

1. L.G.Sillen, Compiler. 'Stability Constants of Metal-ion complexes'. Special Publication no. 17, *The Chemical Society*, London (1964).

2. R.S.Ondrejcin and B.D.Mclaughlin, 'Corrosion of high Ni-Cr alloys and type 304L Stainless steel in HNO_3-HF', Report No. DP-1550(1980), Savannah River Laboratory, Aiken, SC, USA.

3. M.S.Farrell, S.R.Isaacs and M.E.Shying, 'Laboratory Development of the Grind-Leach process For the H.T.G.C.R. Fuel cycle, Pat 2. Dissolution of Beryllia in nitric acid solutions', Report No. AAEC/E154 (June, 1966).

4. M.E.Shying, T.M.Florence and Carswell, 'Oxide Dissolution Mechanisms-1, The Role of fluoride in the Thoria/Nitric/Hydrofluoric acid System', *J.Inorg.Nucl.Chem.* 32(1970):3493-3508.

5. M.E.Shying, T.M.Florence and D.J. Carswell, 'Oxide Dissolution Mechanisms-II, A mechanism for the thoria/nitric/hydrofluoric acid system', *J.Inorg.Nucl.Chem.* 34(1972):213-220.

6. O.K.Tallent et.al., 'The effects of zirconium on the dissolution rate of thoria in nitric-hydrofluoric acid solutions', *Nuclear Technology*, 60(March,1983): 395-405.

Characterization of Deformation Microstructure using Transmission Electron Microscopy: Observation of Cube Slip in γ-TiAl Alloys at Elevated Temperatures

Jung B. Singh

Mechanical Metallurgy Division

Abstract

This article gives a brief description of the use of diffraction contrast transmission electron microscopy for characterizing the deformation microstructure. The capabilities and limitations of different modes of microscopy are also discussed. One of strengths of transmission electron microscopy technique is its capability to identify uncommon deformation system. This is illustrated by the analysis of the cube-slip observed in the deformation microstructure of γ–TiAl alloys at elevated temperatures.

Introduction

Deformation microstructure refers to the microstructural state evolving during a deformation process. The deformation microstructure is characterized by dislocations and other microplasticity elements that participate in the deformation processes, their distribution, their arrangement, density, etc, and, the mechanisms pertaining to their generation. A variety of techniques have been used to study the deformation microstructures at different length scales. These have been mainly [1]: (i) surface relief, which reveals the points of emergence of dislocations at the surface of a crystal; (ii) transmission electron microscopy (TEM), which reveals information at the microscopic level, and is the most commonly used technique; (iii) X-Ray diffraction, in which local differences in scattering are used to reveal the presence of dislocations and (iv) field ion microscopy, which reveals dislocations by the missing atoms and their positions. Recently, scanning electron microscope has also been used to characterize the deformation microstructure by the electron channelling contrast technique [2]. Computational methods have also been employed extensively to predict the deformation microstructure, but they are mostly used as a complimentary technique to assist the analysis of dislocations imaged by TEM. Lastly, dislocation dynamics simulations of plastic deformation have been used to understand dislocation motion, multiplication and their mutual interactions.

The purpose of this article is to give a brief description of the characterization of dislocations using TEM. This technique is best suited for investigating deformation microstructures in materials subjected to only 1 – 2% plastic strain, beyond which the overlapping strain contrast obscure clarity of information. In this article, a brief outline is given first on the different modes of imaging of dislocations in TEM followed by its application to the deformed microstructure of lamellar γ-TiAl alloys that exhibit cube slip at elevated temperatures.

TEM observation of dislocations

Transmission electron microscopy is the most widely used technique for imaging not only dislocations but also other crystal defects such as, stacking faults, twin, grain boundaries, and voids. TEM allows the direct identification of locations of defects, as well as their nature, configuration, etc. The underlying contrast formation mechanism and the imaging

principle are the same for all crystal defects listed above, which basically exploits the effect of their strain fields on electron scattering. For the sake of simplicity, the article is restricted to the imaging of dislocations. Further, the description of contrast and image formation that is presented is, in a strict sense, applicable only to edge dislocations, as they provide a simple illustration of the strains introduced in the crystal lattice.

TEM offers two modes of imaging dislocations based on contrast mechanism employed for their image formation. These two contrast formation mechanisms are (i) phase contrast and (ii) diffraction contrast. The phase contrast mechanism creates a high resolution TEM (HRTEM) image in which columns of atoms parallel to electron beam are

imaged end-on. HRTEM can directly image missing planes and the core structure of dislocations. It can identify planes placed as close as 0.2 nm apart [3]. HRTEM is, however, applicable to a limited number of problems, because it requires dislocation line to be straight and parallel to the electron beam and its core remains same over its entire length [3,4]. HRTEM studies of dislocations are, therefore, mostly limited to dislocations with planar core structures as in the case of covalent crystals and very limited studies are available for metallic materials.

Diffraction Contrast TEM

Diffraction contrast imaging of dislocations exploits the effect of strain fields in Bragg diffraction condition. The presence of a dislocation in a lattice causes atomic planes to bend, particularly at regions
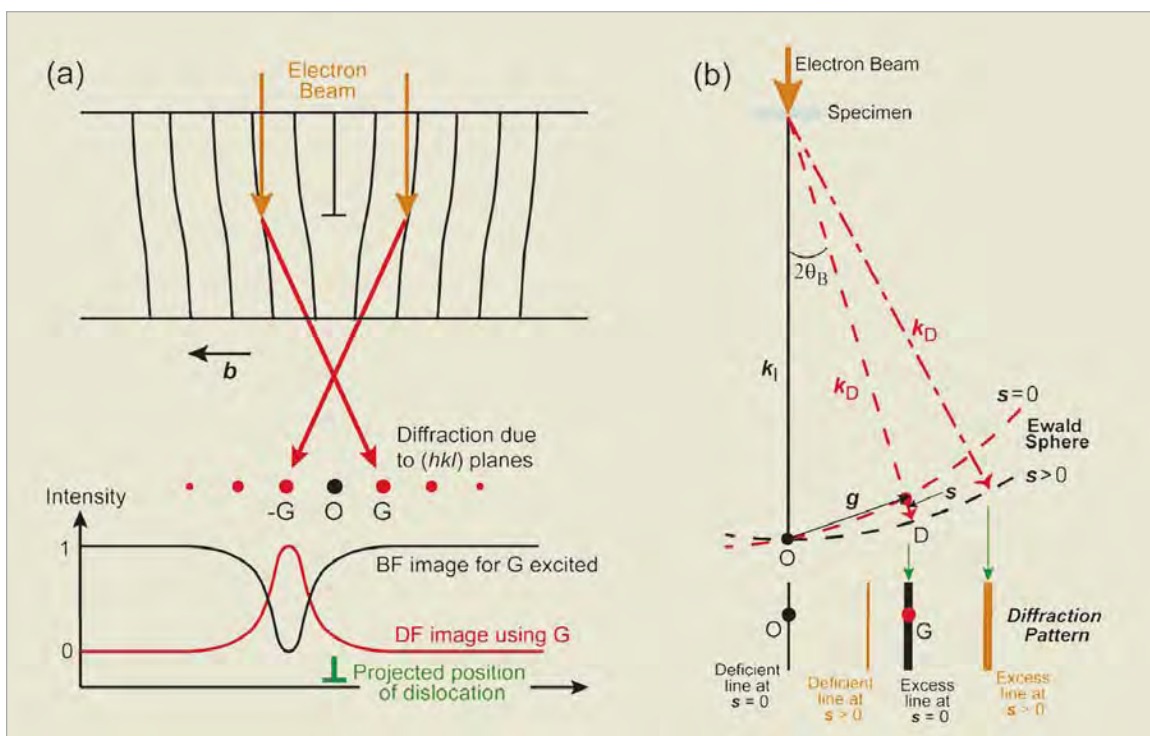
Fig.1: (a) Schematic depicting distorted planes close to the dislocation core diffracting into G and −G. This condition is achieved when the specimen, in general, is tilted slightly away from the Bragg condition ($s \neq 0$) to bring distorted planes near the core into exact Bragg condition ($s = 0$). Lower diagram depicts intensity profiles of the dislocation contrast displaced away from its projected position when imaged with -G reflection. (b) Ewald sphere geometry for two-beam diffraction condition with $s = 0$ and $s > 0$. Lines shown are Kikuchi lines which arise from inelastically scattered electrons [3]. A pair of Kikuchi lines comprises an "excess" and a "deficient" line. These lines help in setting up the Bragg's condition. When s < 0, Kikuchi lines are on the same side of G as O; when s > 0, the lines are on the opposite side of G.

close to the core. For imaging, the specimen has to be first tilted into a two-beam condition, exciting a strong diffraction vector (g) from only a specific set of (hkl) planes, other than the direct (transmitted) beam. It is then tilted slightly away from the exact Bragg condition (i.e. with some excitation error or deviation, $s > 0$) so that distorted planes near the core of dislocation are brought into the Bragg condition while regions distant from the dislocation core are tilted away from it (Fig.1). Some scattered intensity from regions not at the exact Bragg condition may still be visible due to relrods (streaking or broadening of Bragg peak due to size effect). The contrast of dislocation image is determined by $g.R$, where R is the lattice distortion vector. For a pure screw dislocation, R is directly proportional to b. Thus, an analysis of the $g.b$ condition can be correlated to the observed contrast condition of dislocations. Screw dislocations with $g.b = 0$ do not produce any strain contrast, as the diffracting planes are parallel to R. This is known as the "invisibility" criterion for dislocations. For edge dislocations, the condition $g.b{\times}u = 0$ (u is the line direction) also has to be satisfied as the displacement field of an edge dislocation causes buckling of the glide planes. Images formed by diffraction contrast are asymmetric. The location of the diffracted intensity relative to the core depends on the signs of g, b and deviation parameter s. If any sign is reversed, the contrast shifts across the core.

Dislocations can be imaged in two modes, viz., the bright field (BF) or the dark field (DF) mode, depending upon whether the transmitted beam or the diffracted beam is chosen for forming the image. In the BF mode, dislocations appear in dark contrast on a bright back ground, while they appear in bright contrast on a dark background in the DF mode. The dislocation contrast appears only due to the operating diffraction vector and the area that appears dark/bright in the BF/DF images are areas where the hkl planes are at the Bragg condition. TEM analysis of dislocations can determine their b, u, nature

(i.e. edge, screw, or mixed nature) and glide plane. Diffraction contrast imaging can also reveal features such as, jogs or kinks, and the interactions of dislocations with other dislocations or lattice defects. Diffraction contrast imaging has revealed the existence of uncommon defects like stacking-fault tetrahedron, faulted dipoles, and multipoles [3].

Diffraction contrast of dislocations can be obscured by the dynamical scattering of the intense diffracted beam in elastically anisotropy materials. This limits the interpretation and analysis of closely separated dislocations, as in the case of superdislocations of intermetallics. In these cases, the interpretation of the experimentally observed diffraction contrast of dislocations requires the computer simulation of dislocation contrast. Further, the Burgers vectors associated with perfect translations in ordered phases are generally integral multiples of Burgers vectors of lattice dislocations in the corresponding disordered phases (e.g., in Ni_3Al alloys, the perfect dislocations $<110>$ have twice the magnitude of the superpartial dislocations $\frac{1}{2}<110>$). The invisibility criterion, $g.b = 0$, satisfied by dislocations with a Burgers vector b would as well be satisfied by dislocations with Burgers vectors given by an integral multiple of b. Therefore, the invisibility criterion alone cannot be used for an unambiguous determination of the magnitude of the Burgers vector of dislocations in ordered phases. In such cases too, the magnitude of the Burgers vector can be uniquely determined by the computer simulation of dislocation images [see, for example, reference 5].

Diffraction contrast imaging is particularly useful in the in-situ deformation studies, where an understanding of dislocation reactions is required to evaluate the evolution of dislocation structures. Here, miniaturised tensile samples (less than 3mm in gauge length) are strained in the microscope and dislocation movements, dislocation-dislocation interaction, its interactions with other defects and the multiplication processes occurring during the

plastic deformation are observed and recorded in real time. In-situ experiments are a powerful method of studying micro-processes that control dislocation mobility. This technique allows the direct measurement of parameters such as, density of mobile dislocations, kinetics of movements or events, measurement of activation volume. By this technique it is possible to observe metastable core configurations that exist only under stress. Finally, this is the only technique in which the direct observation can be made of processes like dislocations overcoming obstacles such as, precipitates, interfaces, etc. (in succession too).

Weak Beam Transmission Electron Microscopy

WB microscopy is a special case of diffraction contrast imaging in which dislocations are imaged using weakly excited reflections. It is termed weak-beam because the intensity of the diffraction spot employed for imaging is very weak when averaged over the imaging area. The WB condition is obtained by setting the crystal orientation far away from the Bragg condition (i.e., $s >> 0$) in the two-beam condition. Fig.2 schematically depicts a diffraction condition in which the specimen is tilted to a $3g$ WB condition. DF imaging using the G vector in this condition would image dislocations as bright and sharp lines with negligible intensity everywhere else. For WB imaging, the regular two-beam
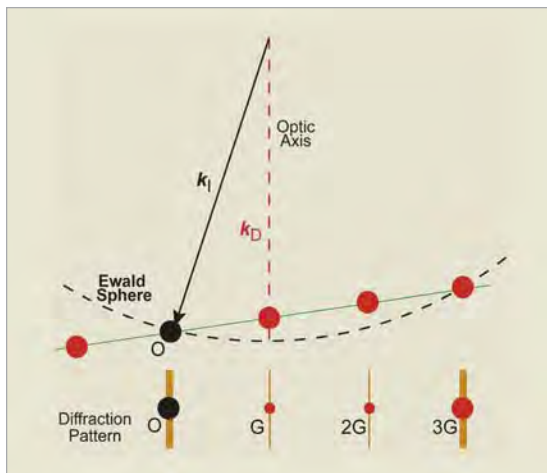

Fig. 2: Ewald sphere and positions of Kikuchi lines for the $3g$ diffraction conditions [3].

condition is first set up and the specimen is then tilted to a large value of deviation, s. As s increases, the average intensity decreases at a rate of $1/s^2$, and the diffraction beam appears as a weak spot [3]. The large s gives a smaller excitation distance and, thus, produces sharp and narrow images of dislocations. Unlike conventional DF imaging, the positions of dislocations imaged under WB are well defined with respect to their cores. The resolution under WB is limited by the minimum volume of crystal (set locally in Bragg orientation) that can cause detectable constructive interference [4]. Using WB imaging, dislocation pairs as close as ~1.5 nm can be resolved [4]. The WB technique is particularly useful for studying finely dissociated dislocations as in intermetallic alloys, where dislocation pairs are separated by very small distances (of the order of nm). In these alloys, superdislocations (e.g., perfect dislocations of the ordered lattice, such as <110> in Ni_3Al alloys) split into two collinear superpartials (with Burgers vectors of ½<110> magnitude for the Ni_3Al alloys) separated by an anti-phase boundary of few nm width. The WB techinique is the only one which can resolve such separations. The other advantages of WB imaging is its low sensitivity to foil thickness and position of dislocations in the specimen, and, lower uncertainties in elastically anisotropic crystals as compared to DF imaging which is affected by dynamical scattering. With the growing interest in applications of intermetallic materials, the WB characterization of dislocations has become popular, as it can resolve fine structures of dislocations in ordered structures (such as, splitting of superdislocations <110> into superpartial dislocations of ½<110>). Such studies have recently led to the discovery of new hardening mechanisms, like the Kear-Wilsdorf lock, operating in ordered structures.

Reliability of the TEM Analysis

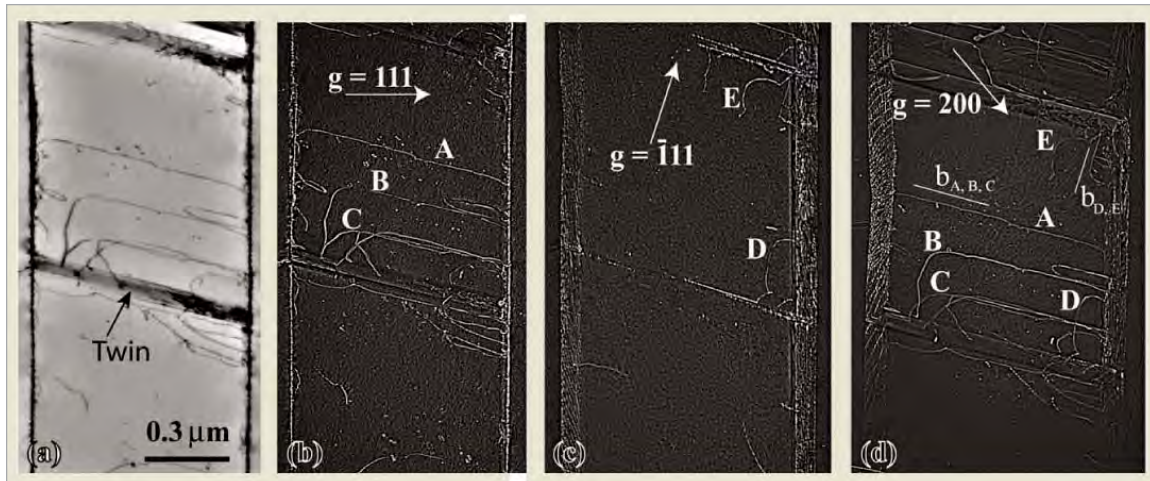Often questions are raised about the reliability of TEM analysis in predicting deformation mechanisms

Fig. 3: (a) BF and (b) to (d) WB micrographs showing dislocations in association with twins in a γ lamella of γ-TiAl alloy deformed at 600°C. Imaging vectors are marked

taking place in bulk material, as a typical TEM sample (i.e., foil region transparent to electron beam) only represents a maximum volume of about 10^{-5} mm^3. A rough estimate of the defect density in TEM samples can be made on the lines of the analysis by Veyssiere [4]. Assume that the density of dislocations contained in a sample deformed to a permanent strain of 1%, is of the order of 10^9 cm^{-2}. This implies that only about a few centimetres of dislocation length can be examined and, out of which, only a small fraction of dislocations are analyzed (i.e., Burgers vector, slip plane, dislocation reaction, etc) to represent the entire deformation process. Despite this extremely limited experimental sampling, the understanding of the bulk deformation microstructure based on TEM investigations is found to be reasonably good and consistent, and has been demonstrated by innumerable independent observations employing different experimental, theoretical and computational techniques. In fact, it can be stated that the understanding in the entire field of dislocations and other crystal defects has advanced principally on account of TEM.

Deformation microstructure of a Deformed γ-TiAl alloy

Most intermetallic alloys, including the engineering wise promising alloys like, Ni$_3$Al, NiAl, TiAl, etc,

are brittle in nature. One of the main reasons for their brittle nature is the insufficient number of independent slip systems available: this is in conflict with the Von Mises criterion which states that five independent slip systems are required for extensive crack-free deformation. However, at elevated temperatures, these alloys generally exhibit improved ductility, partly due to the activation of new slip systems. TEM is the only technique by which one can unambiguously identify the newly activated systems, as is demonstrated in the case of lamellar γ-TiAl alloys described below.

Lamellar γ-TiAl alloys comprise layers of γ-(TiAl - L1$_0$ structure) and α$_2$ (Ti$_3$Al - D0$_{19}$ structure) phases stacked along the (111)$_\gamma$ plane such that the two phases follow $(111)_\gamma // (0001)_{\alpha_2}$ and $<1\bar{1}0]_\gamma // <1\,1\bar{2}0>_{\alpha_2}$ orientation relationships. (The $<uvw]$ mixed bracket notation denotes that all permutations of u and v indices are allowed while the third index is fixed [6]). These alloys contain γ lamellae in a much higher number and volume fraction than α$_2$ lamellae. The α$_2$ phase forms in one orientation, while the γ-phase can take six different orientations as described elsewhere [7]. As a consequence, three different types of γ/γ interfaces (namely, ordered domain related, pseudo-twin related or true-twin related [7]), in addition to a γ/α$_2$ interface, can form within a grain.
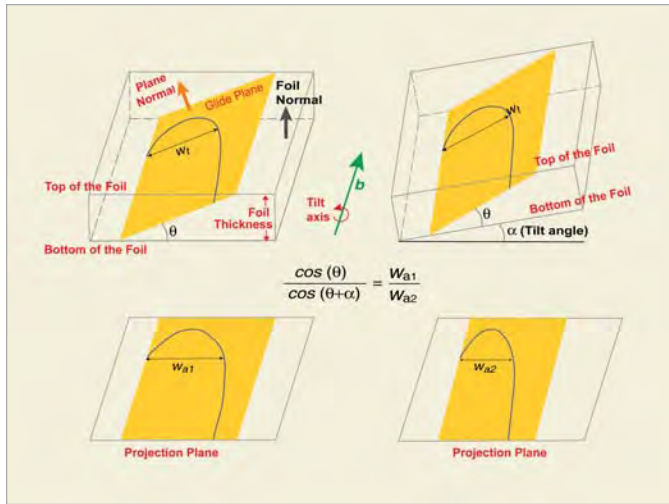
Fig. 4: Schematic illustrating the determination of habit plane of dislocation using tilt experiments.

Dislocations can easily transfer across true-twin related interfaces since there is always a slip system in mirror symmetry in an adjacent twin-related γ lamella. Spreading of strain across mismatched (ordered domains or pseudo-twin) interfaces often violates the Schmid law, as internal stress concentrations due to dislocation pile-ups in the source lamella is the main deciding factor. Strain transfer across α_2 lamellae occurs mainly through the effect of elastic strain field, which activate sources in neighbouring γ lamellae [8]. Since microstructure in a polycrystalline lamellar γ-TiAl alloys is dominated by true-twin related γ/γ interfaces [7], deformation within γ lamellae and its transfer across interfaces plays a major role in the observed macroscopic plasticity. Deformation within a γ-phase is achieved by the propagation of ordinary dislocations (e.g., $1/2<1\bar{1}0]$, $1/2<101]$) or superdislocations ($1/2<11\bar{2}]$) dislocations. Twinning is also observed, especially at elevated temperatures. As per the underlying symmetry conditions, deformation is first initiated in γ lamellae on the basis of Schmid factor considerations, which then propagates to adjacent lamellae that are in true-twin relationship.

Fig. 3 shows the deformation structure of a γ-lamella: twins can be seen in addition to ordinary dislocations. The details of these experiments are available elsewhere [7]. The observed twins are determined to be true twins. The stereographic analysis of the twins reveals that they lie on the $(\bar{1}11)$ planes. The Burgers vectors of the dislocations were determined by the invisibility criterion. The dislocations A, B and C have $\frac{1}{2}[110]$ Burgers vector, while dislocations D and E have $\frac{1}{2}[1\bar{1}0]$. Stereographic analysis confirms that they are screw dislocations. These dislocations can be contained in more than one plane. For instance, dislocations with Burgers vector $\frac{1}{2}[110]$ may lie on one of the $(\bar{1}11)$, (001), $(1\bar{1}1)$ or $(\bar{1}10)$ planes. As schematically illustrated in Fig.4, the exact plane that the contains the dislocations is determined from their projected width in the projection plane (image plane). If W_a is the apparent width of a dislocation lying on a plane (hkl), then it's true width, W_t would be given by

$$W_t = \frac{W_a}{\cos \theta} \qquad (1)$$

Where, θ is the angle between the beam direction and the (hkl) plane normal. If the apparent widths of a dislocation at two foil orientations are W_{a1} and W_{a2} measured at foil rotation angles θ_1 and θ_2, then

$$\frac{W_{a1}}{W_{a2}} = \frac{\cos \theta_1}{\cos \theta_2} \qquad (2)$$

This implies that the ratio of the apparent widths at two foil orientations would be same as that of the ratio of cosines of the angles between the beam direction and the plane normal.

Using the relation (2), the actual plane containing dislocations A, B and C is identified. Dislocations are imaged using the $g = 220$ reflections and the specimen is rotated through –30° to 30° around the Burgers vector. Fig.5 shows two images of this tilt series, one with the sample tilted by –23° and
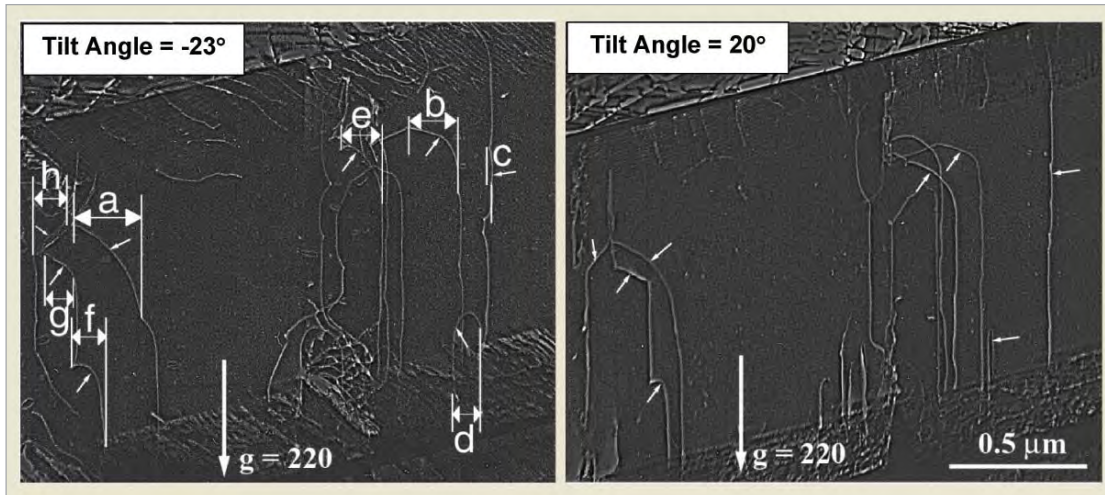
Fig. 5: WB analysis of planes containing dislocations. The habit planes of segments a to h are identified (see text for details)

the other tilted by +20°. The habit planes of 8 segments, namely **a**, **b**, **c**, **d**, **e**, **f**, **g** and **h**, are analysed from their apparent widths measured perpendicularly to the tilt axis. Angular measurements are done with an overall uncertainty of ±4° (arising as ±2° from the goniometer and as ±2° from the stereogram used for measurements), while width measurements are done with an uncertainty of ±0.04 μm. Table 1 gives list of possible planes that can contain these dislocations along with angles (measured by stereographic analysis) they make with the foil normal. The right

hand side of the table list the ratio of projected widths of these segments imaged at −23° and +20° tilt conditions. From a comparison of the ratio of cosine angles with that of projected widths, it can be noticed that the segment **c** lie on ($\bar{1}$11) (nearly edge-on in Fig.5b) while segment **h** is on (001). Segments **d** and **b** are in planes rather close to ($\bar{1}$11) and (001), respectively while segments **a**, **e**, **f** and **g** lie on planes all located much closer to the (001) plane than to any of the other crystallographic planes considered in the vicinity of (001). This established unambiguously the activation

Table 1: Possible planes that can contain dislocation segments analysed in Fig.5

Possible Planes	Angle between Foil Normal and Plane Normal	$\dfrac{Cos_{-23°}}{Cos_{+20°}}$	Dislocation Segment	$\dfrac{W_{a-23°}}{W_{a+20°}}$
(001)	+22°	1.35 ± 0.07	a	1.07 ± 0.04
			b	1.17 ± 0.05
($1\bar{1}1$)	-46°	0.54 ± 0.08	c	8.0 ± 5.0
			d	$6.0^{+2.3}_{-1.4}$
($\bar{1}11$)	+75°	8.83^{+30}_{-10}	e	0.91 ± 0.04
			f	1.87 ± 0.02
($1\bar{1}0$)	-68°	0.03 ± 0.10	g	$1.04^{+0.07}_{-0.01}$
			h	$1.38^{+0.12}_{-0.11}$

of (001) slip of ordinary dislocations thus providing an extra slip system for deformation at elevated temperatures.

Conclusions

Transmission electron microscopy provides the most detailed analysis of the nature of dislocations and the deformation behaviour. It is the only tool that can reveal uncommon slip systems and deformation processes that often occur in many alloy systems that are currently under development for structural application for high temperature service. No other technique can match its imaging capabilities– the others may only compliment it by sampling larger volumes of the specimen.

Acknowledgements

References

1. D. Hull and D.J. Bacon: Introduction to Dislocations, Fourth Ed., 2001, Butterworth Heinemann, OX, Chap.2.

2. X.W. Li: Direct Characterization of Various Deformation Microstructures in Metals by Electron Channeling Contrast Technique in SEM, *Advanced Materials Research*, Vols. 79-82 (2009,) pp 215-218.

3. D.B. Williams and C. B. Carter: Transmission Electron Microscopy, Second Ed., 2009, *Springer Science*, NY, vol.3.

4. P. Veyssier: Weak-beamTransmission Electron Microscopy Analysis of Dislocation *Processes in Intermetallics, ISIJ International*, Vol. 31 (1991), 1028.

5. J.B. Singh, M. Sundararaman and P. Mukhopadhyay: Propagation of Stacking Faults across Domain Boundaries in Ni-V and Ni-V-Nb Alloys with $D0_{22}$ Structure, Philos. Mag. A, vol. 80 (2000), 1983.

6. G. Hug, A. Loiseau and P. Veyssiere, Philos. Mag. A, vol. 57 (1988), 499.

7. J. B. Singh, G. Molenat, M. Sundararaman, S. Banerjee, G. Saada, P. Veyssiere and A. Couret: The activation and the Spreading of Deformation in a Fully Lamellar Ti–47at.%Al–1at.% Cr–0.2at.% Si Alloy, Philos. Mag., vol. 86 (2006), 2429.

8. J. B. Singh, G. Molenat, M. Sundararaman, S. Banerjee, G. Saada, P. Veyssiere and A. Couret: In-situ Straining Investigation of Slip Transfer across α_2 lamellae at room temperature in a Lamellar TiAl Alloy, *Philos. Mag. Lett*, vol. 86 (2006), 47.

Early Detection of Coronary Heart Disease Using Peripheral Pulse Analyzer

G.D. Jindal, R.K. Jain, Vineet Sinha, Sadhana A. Mandalik,

Bhagyashree S. Sarade, Pooja Tanawade and C.K. Pithawa

Electronics Division

and

Prasanna M. Kelkar

Ayurved Hitaishani Trust and Samshodhan Kendra,

Thane (W), India

and

Alaka K. Deshpande

Department of Medicine, Grant Medical College and JJ Hospital, Mumbai, India

Abstract

Electronics Division, Bhabha Atomic Research Centre has developed a Peripheral Pulse Analyzer for early detection of coronary heart disease. The instrument employs the principle of impedance plethysmography and measures electrical impedance and its time derivative (representing blood flow) at three consecutive segments on the wrist of the human. In view of our earlier observation that some apparently normal subjects have recorded abnormal impedance plethysmogram from the chest and have suffered heart attack in subsequent 20 years, the peripheral plethysmograms have been analyzed in around 300 subjects. It has shown 8 dominant morphological patterns of the peripheral pulses depending upon their status of health. In cognizance of these observations, a Fourier Transform based method has been developed and incorporated with the instrument to obtain Morphology Index (MI) of the peripheral pulse. The index varies from 0 to 1, the former indicating the poorest and later the complete health. These observations are corroborated by variability spectrum of heart rate and peripheral blood flow. The average index is observed to be around 0.3 in patients with myocardial infarction. Early stages of coronary artery disease bring down the index to around 0.4. Thus it is possible to detect coronary artery disease in early stages.

Keywords: Impedance Plethysmograph, Peripheral Pulse Analyser, Pulse Morphology, Morphology Index, Predictive Diagnosis.

Introduction

Bhabha Atomic Research Centre (BARC) developed 1st model of Impedance Plethysmograph (IPG) in 1978 and installed at Department of Surgery, Seth G.S. Medical College & K.E.M. Hospital and Department of Medicine, Grant Medical College & J.J. Hospital, Mumbai for the assessment of central and peripheral blood flow in the human body. Extensive clinical trials on 103 normal subjects and 10,000 patients with peripheral vascular occlusive diseases at KEM Hospital during 1978 to 1990 and comparison of IPG observations with angiography observations in large number of 500 subjects revealed the sensitivity and specificity of this indigenously developed technique to be 96% and 98% for the diagnosis of peripheral arterial occlusive disease [1] and more than 80% for the diagnosis of deep vein thrombosis [2].

Impedance Plethysmograms of the thoracic region, commonly known as Impedance Cardiograms (ICG), recorded in control subjects at JJ Hospital have shown different morphological patterns (Fig 1). In a group of 103 subjects, without any demonstrable cardio-vascular disorder, type-A, type-B, type-C and type-D waveforms were recorded in 67, 14, 9 and 13 subjects respectively by Deshpande et al (1990). Estimation of hemodynamic parameters are considered to be reliable in type-A and type-C

waveforms as the B-point, maker of the opening of aortic valve, is clearly discernible in the waveform and all measurements (PEP, LVET) can be made with respect to this point. Type B waveform is otherwise recorded in subjects aging more than 40 years, obese or those with systemic hypertension. However computation of LVEF etc. becomes difficult/ ambiguous in such cases as B-point is not well defined. Type–D waveform recorded from 13 normal subjects, by no means, can be classified as normal waveform as similar pattern is recorded in patients with tricuspid regurgitation and those with myocardial infarction. Though B point is distinctly seen in this waveform, LVEF obtained from this category is significantly lower. In the absence of clinical correlation, these cases have been regarded as false positives. ***It is interesting to mention that all the subjects in this group of 13 have suffered heart attack during subsequent 15 years.*** *This suggested predictive diagnostic potential of this technique.*

The IPG instrument has undergone several renovations during the past 31 years such as microprocessor based impedance plethysmograph,

introduction of simple and reliable calibration for dZ/dt waveform [3], Correction of formula for estimation of peripheral blood flow [4], introduction of normalized dZ/dt waveform for easy assessment of peripheral blood flow [5], PC based impedance cardiovasograph system [6] and variability analysis [7].

The variability analyzer developed at BARC records peripheral blood flow from the wrist location of the subject for a period of 300 seconds and yields short term variability in heart rate (HRV) and peripheral blood flow (PBFV) which is not available with any other commercial instruments. Preliminary study carried out on 300 subjects at JJ Hospital has shown the effect of several diseases on the variability spectrum of these parameters. Such changes in HRV have already been correlated to peripheral neuropathy in diabetic subjects [8] and other cardio-vascular ailments [9].

Fig. 2 shows the heart rate variations in time and frequency domain in a control subject. It is difficult to analyze these variations in time domain as several rhythms are simultaneously causing them. However, Power Spectral Density (PSD), obtained by Fast

Fig. 1: Variation in the morphology of ICG waveforms in subjects without any demonstrable cardiovascular disorder. B-point, indicated by the arrow, is clearly discernible in type-A and type-C waveforms recorded from 73.8% of the presumably normal subjects. However 26.2% of the subjects have recorded waveforms with morphologies similar to that of type-B or type-D. The waveforms of latter types invariably caused inaccuracy in the computation of hemodynamic parameters

Fig. 2: Typical heart rate fluctuations in time (lower) and frequency domain (upper) in a normal subject

Fourier Transform (FFT) of the same, isolates different rhythms distinctly. There are three distinct peaks observed in the frequency domain centred around 0.008, 0.106 and 0.213 Hz, commonly known as Very Low Frequency (VLF) peak, Low

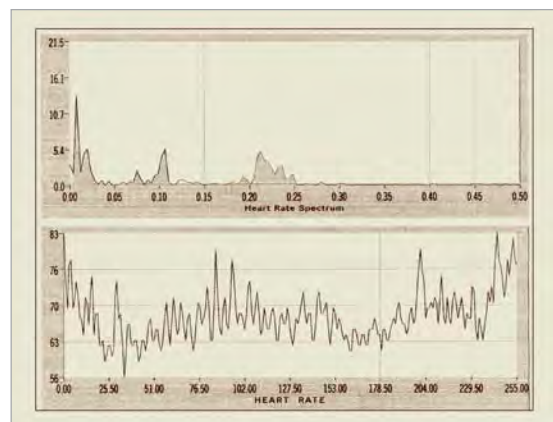Frequency (LF) peak and High Frequency (HF) peak respectively. Though the origins of these peaks are not clearly understood, it is in general agreed that VLF is contributed by baro-receptor reflex/ renin-angiotensin system; LF is contributed by sympathetic and para-sympathetic nervous system and HF is contributed by vagal slowing part of para-sympathetic system.

Fig. 3 shows similar data in a patient with pulmonary tuberculosis. The difference in variability spectrum can be well appreciated. Fig. 4 shows the variability spectrum of blood flow index in a control subject (top) and in a patient suffering from AIDS (bottom). The difference between the two spectra is obvious. To converge these findings in to a diagnostic tool, multi centric clinical research is in progress.
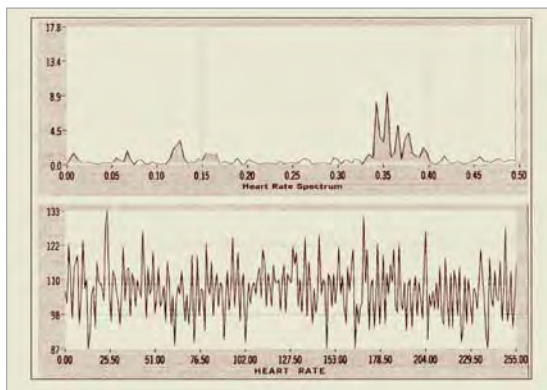
Fig. 3: Typical heart rate fluctuations in time (lower) and frequency domain (upper) in a patient suffering from pulmonary tuberculosis
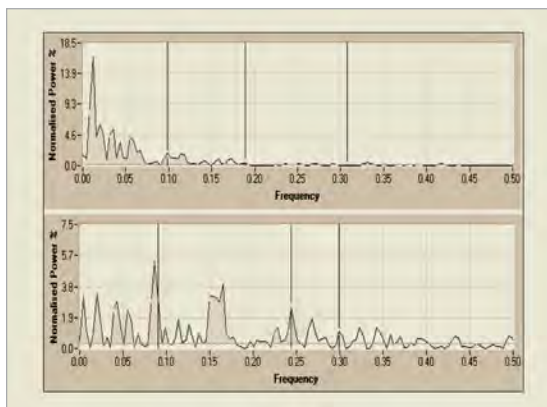
Fig. 4: Typical blood flow index fluctuations in frequency domain in a control subject (upper) and in a patient suffering from AIDS (bottom)

While analysing variability Analyzer data, it has been noticed that the morphology of the blood flow pulse varied as a function of time in a given individual and also from individual to individual. It is observed that in a span of 300 seconds an individual has a dominant pattern most of the time with other patterns interposing intermittently. A closer examination of the data in all the 300 subjects has revealed that all the pulse patterns could be classified into 8 basic morphologies as shown in Fig. 5. Top left is the pulse morphology, commonly observed in normal subjects and bottom right is the pulse morphology, commonly observed in patients with severe coronary artery disease.
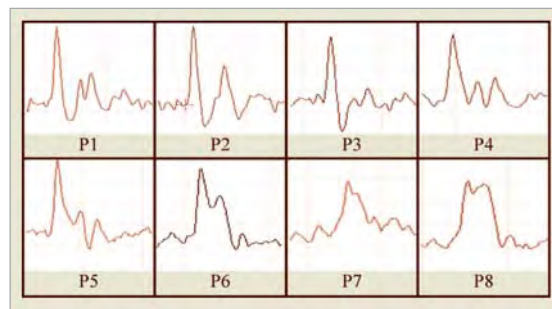
Fig. 5: Eight Basic Morphological Patterns of Peripheral Pulse

In order to assign a numerical value to pulse pattern, named as Morphology Index (MI), K-Factor and Fisher's ratio have been used by others in the past and have met partial success. Closer examination of short term FFT of peripheral pulse has revealed significant difference between spectra of various morphologies. Since data of one cardiac cycle gives poor resolution due to limited number of samples, 511 samples on the left side and 512 samples on the right side of the peak are given as input for short term FFT for higher resolution as shown in Fig. 6. The morphology index (MI) is computed from the FFT data using following formula:

$$MI = \frac{\sum_{i=6}^{i=127} PSD(i)}{\sum_{i=2}^{i=127} PSD(i)}$$

where, *PSD(i)* is the sum of squares of real and imaginary Fourier co-efficient as obtained from FFT.
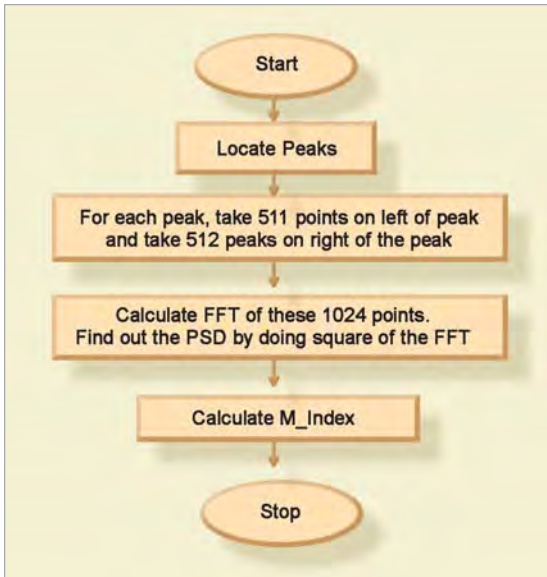
Fig. 6: Flow chart for calculation of MI

The first two co-efficient are ignored as they represent the DC component. Fig. 7 shows the peripheral pulses and their short term FFT. Only 32 co-efficients are shown for the purpose of clarity. For morphology pattern 1, the high frequency components are dominant with the result the MI is closer to unity. Whereas, for morphology pattern 8, the lower frequency components are dominant with the result that MI is approaching towards Zero. The other patterns are having values between 0 and 1. Data analysis based on Morphology Index has shown that normal subjects record patterns 1,2 and 3 predominantly with brief interpositions of pattern

4 to 8. Patients suffering from disorders of Lungs, Liver and Heart record patterns 5 to 8 predominantly with brief interpositions of pattern 1 to 4. Patients with beginning of ischemic heart disease show pattern 6 and 7 with occasional interposition of pattern 8, where as those with myocardial infarction show pattern 8 predominantly provided the patient is not on heavy dose of aspirin or beta blockers.

Peripheral Pulse Analyzer

In view of above, an instrument named as Peripheral Pulse Analyzer, incorporating all the features described above, has been developed at Electronics Division BARC. It comprises a sine-wave oscillator, voltage to current converter, three sensing amplifiers along with analog processing circuits, a low power micro-controller and a Bluetooth controller communicating with a personal computer as shown in Fig. 8. A fixed amplitude sinusoidal current (2 mA) is passed through the upper extremity by applying carrier electrodes C1 and C2 around elbow and palm. The voltage developed along the current path is sensed from three locations at the wrist with the help of sensing electrodes S1-S4, with S1 proximal to elbow and S4 to the palm. The inter-electrode distance between S1 to S4 is kept around 2 cm. The voltage differences between S1 and S2; S2 and S3; and S3 and S4 are amplified with the help of sensing amplifiers (1) to (3) respectively.
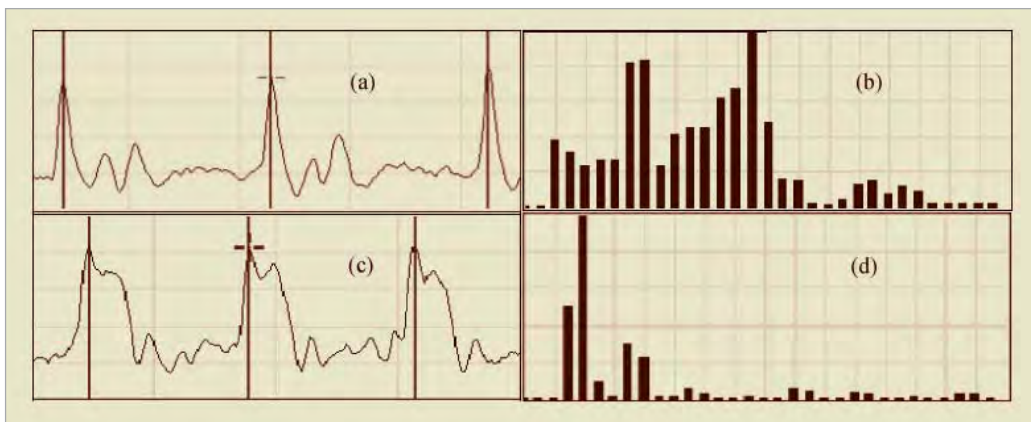
Fig. 7: Shows the peripheral pulse recorded from a normal subject (a) and a patient with severe coronary artery disease (c). The short term FFT is given in (b) and (d) respectively
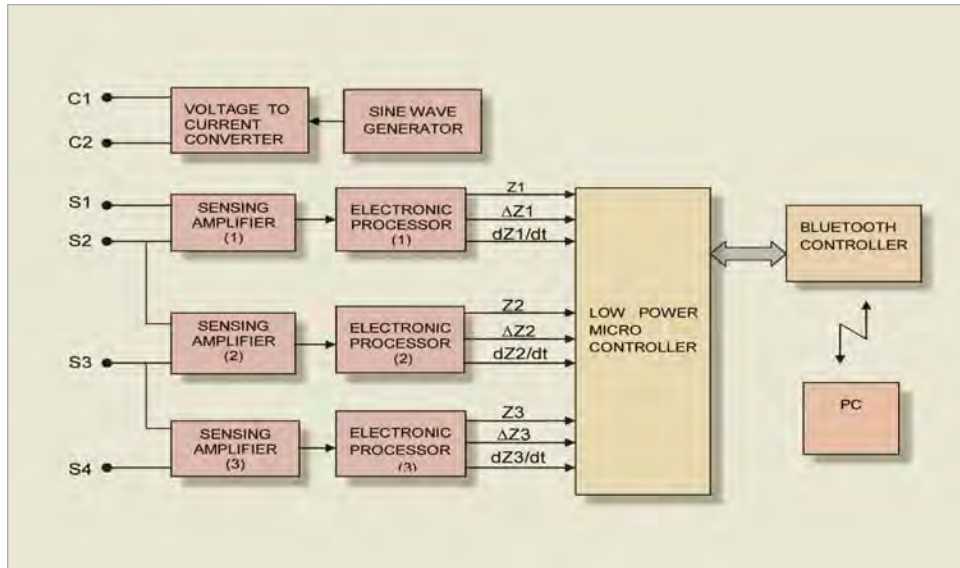
Fig. 8: shows the schematic diagram of the Peripheral Pulse Analyzer developed at Electronics Division BARC

These locations on the wrist correspond to Vata, Pitta and Kapha locations of Ayurvedic System of Medicine. The amplified signals are further processed to yield impedance of the segment (Z1 to Z3); change in impedance with time meaning difference of instantaneous impedance Z(t) and initial impedance Z_0 (DZ1 to DZ3); first time derivative of impedance (dZ1/dt to dZ3/dt) representing body composition; blood volume change; and blood flow in the respective segment respectively. These signals are connected to ADC inputs of the micro-controller as shown in the Fig 8. These signals are acquired at a rate of 500 samples per second and communicated to personal computer through Bluetooth controller for further processing and analysis. Fig. 9 shows the photograph of the instrument along with personal computer.

The firmware includes acquisition of all the user selected signals at selectable rate and sending to PC through Bluetooth controller. The application software has two parts; acquisition and processing, described elsewhere [10]. During acquisition, after entering the personal data and basic settings for the subject, click on AQUIRE button starts data acquisition till the same button is re-clicked or 275

Fig. 9: Peripheral Pulse Analyzer in action

seconds have elapsed, whichever is earlier. At the end of acquisition, the data is saved in the prescribed file format. Also the file can be converted to ASCII format and saved for processing on other software packages. For processing the file, the patient data is loaded by clicking on LOAD, signals are selected for processing and SELECTION PANEL is clicked. Cursor is placed on third systolic peak in dZ3 (dZ3/dt is abbreviated as dZ3) and LOCATE PEAK is clicked. This automatically highlights all the systolic
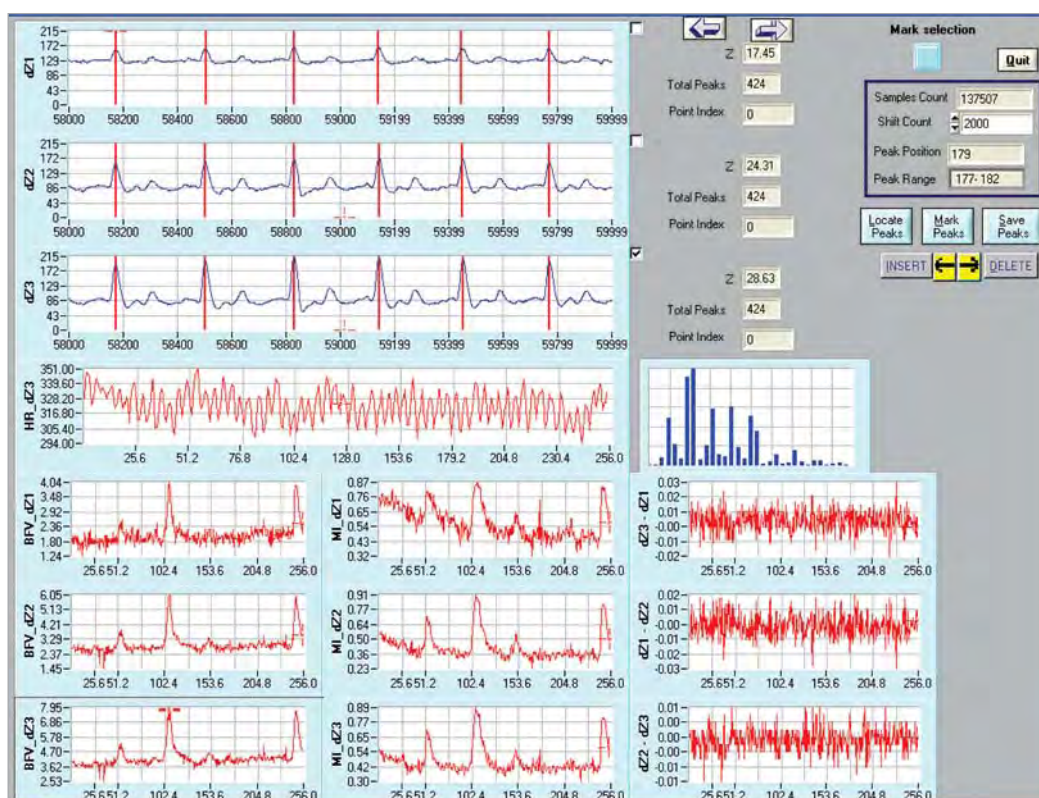
Fig. 10: The selection panel during processing of the data, displaying variability of various parameters in time domain and short term Fourier Transform of a particular data segment

peaks in the signal. Any discrepancy in peak selection shows up on the 4th graph (from top), labelled as HR_dZ3 in the panel, which can be manually edited by using INSERT, DELETE, SHIFT LEFT and SHIFT RIGHT buttons. A click on MARK PEAKS plots all the graphs below and those on the right showing variations in blood flow, morphology index and pulse travel time in time domain for all the dZ (dZ/dt abbreviated as dZ) signals as shown in Fig. 10. These are labelled as 'BFV_dZ1, BFV_dZ2, BFV_dZ3, MI_dZ1, MI_dZ2, MI_dZ3, dZ3-dZ1, dZ1-dZ2 and dZ2-dZ3' respectively. Any spurious spike is manually edited using the above described buttons. The selected peak information is then saved in the file.

As can be seen from the Fig.10, MI_dZ3 shows wide variation in the morphology of the pulse ranging from 0.30 to 0.89. The short term FFT shown in the graph by the side of HR_dZ3 graph is for the peripheral pulse for MI equal to 0.89. The corresponding pulse pattern can be seen in the graph

labelled dZ3, which resembles pattern P1. One can also get the average morphology index for the subject by quitting this panel and going to DISPLAY panel, where the variability is shown in frequency domain.

The instrument has been used for screening nearly 100 subjects suffering from various disorders. Consistently those suffering from coronary heart disease have recorded patterns P6 to P8, with average morphology index ranging from 0.3 to 0.45. Multi-centric trials are in progress at Grant Medical College & J.J. Hospital, Mumbai; Ayurved Hitaishani Trust; Samshodhan Kendra, Thane; Father Muller Medical College, Mangalore; and Arya Vaidya Sala, Kotakkal.

Acknowledgements

Shri Ashok D. Kamble in data collection and processing.

References

1. Jindal GD, Nerurkar SN, Pednekar SA, Babu JP, Kelkar MD, Deshpande AK and Parulkar GB, *Diagnosis of peripheral arterial occlusive diseases using impedance plethysmography*, J. Postgrad. Med. Vol. 36, p.147, 1990.

2. Jindal GD, Pedhnekar SA, Nerurkar SN, Masand KL, Gupta DK, Deshmukh HL, Babu JP and Parulkar GB, *Diagnosis of venous disorders using impedance plethysmography*, J. Postgrad. Med. Vol. 36, p.158, 1990.

3. Jindal GD, Babu JP, *Calibration of dZ/dt in impedance plethysmography*, Med. Biol. Engg. & Comput. Vol. 23, p. 279, 1985.

4. Jindal GD, Nerurkar SN, Pednekar SA, Babu JP, Kelkar MD and Deshpande AK, *Corrected formula for estimating peripheral blood flow by impedance plethysmography*, Med. Biol. Engg. Comput. Vol. 32, p.625, 1994.

5. Jagruti C, Chaugule N, Ananthakrishnan TS, Prakash Babu J and Jindal GD, *Normalized DZ/DT waveform for easy assessment of peripheral blood flow*, Proc. SBME-NM 2000, p.67, 2000.

6. Jindal GD, Ananthakrishnan TS, Kataria SK and Deshpande AK, *An Introduction to Impedance Cardiovasography*, External Report, BARC/2001/E/003, 2001.

7. Jindal GD, Ananthakrishnan TS, Mandlik SA, Sinha V, Jain RK, Kini AR, Nair MA, Kataria SK, Mahajan UA and Deshpande AK, *Medical Analyzer for the study of physiological variability and disease characterization*, External Report, BARC/2003/E/012.

8. Bianchi A, Bontempi B, Cerutti S, Gianoglio P, Comi G and Natali Sora MG, *Spectral analysis of heart rate variability signal and respiration in diabetic subjects*, Med. and Biol. Eng. and Comput., Vol. 28, pp 205-211, 1990.

9. Marek Malik, *Clinical Guide to Cardiac Autonomic Tests*, Kluwer Academic Publishers, 1998.

10. Jindal GD, Deepak KK and Jain RK, *A Handbook on Physiological Variability*, Proceedings, Theme Meeting on Advanced Applications of Physiological Variability – 2010, BARC, Mumbai.

Development of Fluidized Bed Thermal Denitration

Neetu A. Baveja, C.P. Shringi, Gaurav Varshney, Deepa Thomas,
Sandip Bhowmick, N.K. Dandekar, M.Y. Walke and Hanmanth Rao
Chemical Engineering Division

Abstract

Nitrate streams generated in the front-end and back-end of nuclear fuel cycle, require denitration for conversion of product streams as oxide for fuel fabrication or long term storage and for disposal of waste raffinate streams with minimum environmental impact. This also helps in recycling of nitric acid. Chemical Engineering Division has been involved in the development of thermal denitration in a fluidized bed which is having high wall to bed heat transfer coefficient, continuous processing capability and ease of control. The Division has gained operating experience with synthetic magnesium nitrate and ammonium nitrate streams in a bench scale facility of 5 lph capacity. The experience has been used for setting up of a pilot plant of 30 lph capacity, which has been used for optimization studies on denitration of ammonium nitrate solution. The paper shares the operating experience gained with the nitrate streams in bench scale and pilot plant facilities.

Keywords: *Fluidized Bed Denitration; Fluidization*

Introduction

The process of fluidized bed thermal denitration consists of atomization of the nitrate solution into fine droplets onto a bed of fluidized particles maintained at high temperature. The solution gets coated on a small fraction of particles which mix with the rest of the bed. The solute forms a layer that coats the bed particles and subsequently gets dried and calcined. Water vapor and gaseous decomposition products are removed from the bed with the fluidizing gas. The solid part of the bed may be continuously removed as product, by maintaining constant solid volume inside the bed. Thus the decomposition process can be continuous and does not require any addition of chemicals. Air is used to achieve fluidization of the particles and as atomization gas in the feed nozzle. Heat is furnished to the fluidized bed by induction heating system.

Denitration Facility in the Division

A bench scale facility for fluidized bed thermal denitration has been setup at CEL III, BARC. The plant has a capacity of 5 lph of nitrate solution and uses a denitration column of 150 NB. Denitration studies with synthetic magnesium nitrate and synthetic ammonium nitrate solutions have been carried out.

Based on the experience obtained in the bench scale facility, a pilot plant which has 300 NB denitration column has been set up and successfully commissioned.

Denitration plant can be divided into four major sub systems: Solid handling system, feed system, heat supply system and off gas system. Fig. 1 shows a typical block diagram for the denitration facility at CEL III.

Solid Handling System

Continuous feeding and withdrawal of solids from the denitration column is required to maintain particle size distribution inside the bed for achieving good hydrodynamics suitable for high heat transfer. This requirement could be met in the set up by using non mechanical feeding and withdrawal systems.
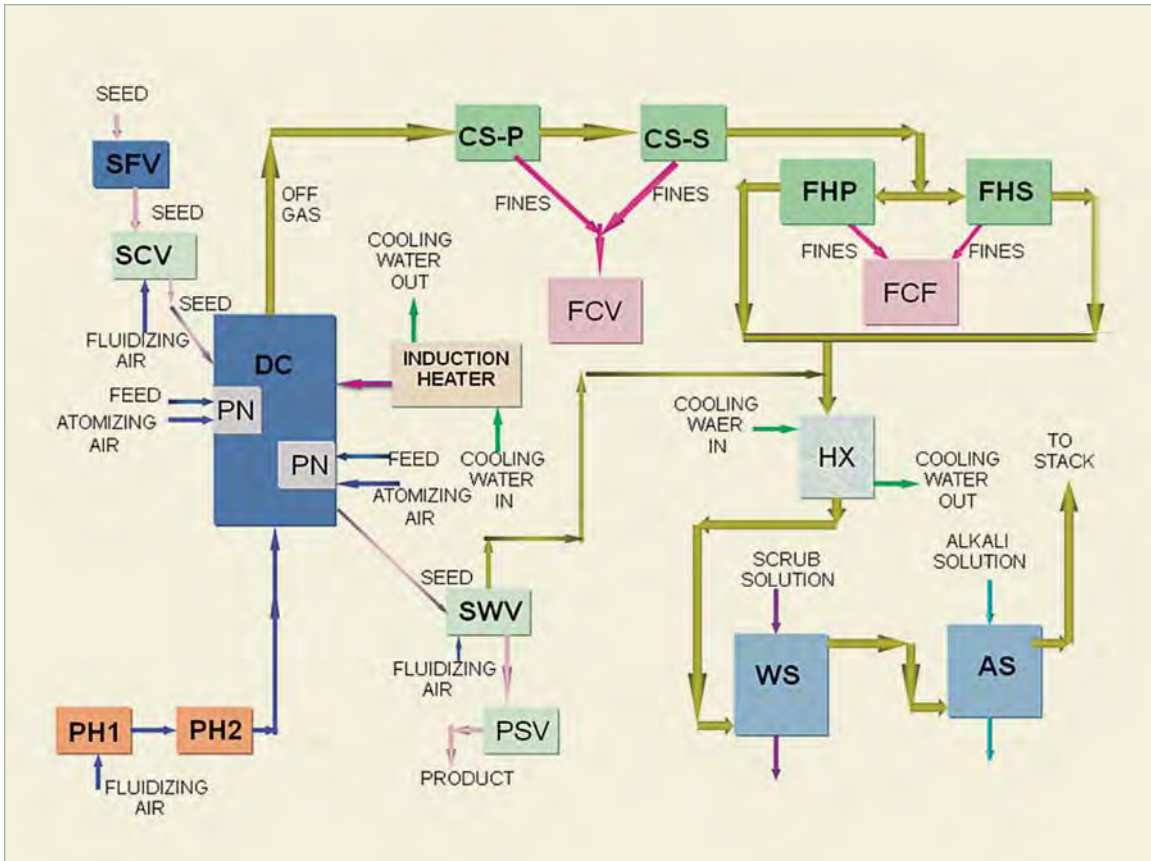
Fig. 1: Typical Block Diagram for Denitration plant

The seed material is continuously fed to the denitration column (DC) using a non-mechanical solid feeder. Solid flow through a non mechanical valve / feeder can be varied by varying aeration flow through the same. Bed height in the denitration column is maintained constant by continuous withdrawal of the seed through a bed level actuated feed back control loop through a non-mechanical solid withdrawal system (SWV and PSV). Withdrawn seed is separated from the product continuously and fed to the solid feeder (SFV and SCV). Seed material used inside the DC is product itself in case of product streams and some inert material for waste streams.

A sparger pipe is used for primary distribution of fluidizing air which then passes through a perforated plate distributor. The level inside the bed is measured by using a differential pressure transmitter and temperature at various axial and radial locations are

measured using K type thermocouples. Freeboard section provided at the top has twice the diameter of the bed.

Feed System

Synthetic nitrate solution has been used as feed stream. The feed solution along with the atomizing air is fed continuously to the denitrator through externally mixed, pneumatic spray nozzles (PN) placed inside the bed.

Pneumatic spray nozzles, which use air as atomizing medium, have less tendency of getting choked, and can also produce small droplet size with a narrow spectrum as per process requirement. Externally mixed type of nozzle is selected for the set up because liquid and air streams can be independently controlled. Passive spray nozzles are used in the column which can be automatically put on line if the active one gets choked.

Metering pumps having electronic stroke control mechanism is used for transferring the feed to the denitrator. Pulsation at the discharge of the pump is dampened to $\pm$ 1 % of the average flow using a dampener.

Heat Supply System

Electric induction heating capable of providing high watt-density is used to maintain the desired temperature inside the bed. Fluidizing air is preheated using electrical heaters (PH1 and PH2).

Off Gas System

Entrained solid product is removed using cyclone separators (CS-P and CS-S) and sintered metal filters (FH). Condensed water vapor containing absorbed NOxHNO$_3$ solution is obtained from the condenser (HX). Gas is then passed through water scrubber (WS) for further nitric acid recovery. Remaining traces of NOx are removed in alkali scrubber (AS). The gases are released through the stack after adequate dilution meeting the gas emission norms.

Operating Experience in the Bench scale facility

Blank (with water as feed) runs were initially carried out for performance evaluation of various sub systems in the plant. Continuous solid circulation could be established and constant bed level in the denitration column was obtained. Circulation rate could be varied within a wide range, however for the nitrate feed runs the rate was kept in the range of 3 – 15 Kg / hr.

The column has one active feed nozzle and one passive feed nozzle. Passive nozzle can be used if the active one gets choked during operation. Metering pump with dampener system performed satisfactorily and smooth and continuous flow could be achieved. Pneumatic spray nozzles used for feeding performed smoothly and operation could be on-line changed from one nozzle to the other.

Initially electrical resistance heaters made from nichrome wire covered with ceramic beads were used as heat source. These heater coils were wrapped externally around the denitration column. Heat input to the bed is controlled by using PID control which takes input from one of the thermocouples placed inside the bed. There are 10 thermocouples for measurement of bed temperature and 2 thermocouples for measuring wall surface temperature. Additionally two thermocouples are provided for measurement of freeboard temperature and 1 for freeboard surface temperature. Uniform temperature profile and high heat transfer coefficient (500 – 700 W/ m^2 K) could be achieved inside the bed. A representative temperature profile observed inside the column during denitration studies is shown in Fig. 2

Later induction heater was used as heat source to the column. This heater was found to be more robust and reliable than the electrical resistance heater.

Experience with Magnesium Nitrate Solution

Magnesium nitrate solution was used for process feasibility study because it has chemical and decomposition properties similar to Uranyl nitrate solution generated in the nuclear fuel cycle. In the initial nine runs, electrical resistance heat supply system was used externally to provide process heat. These runs were taken with feeding carried out using downward facing spray nozzle placed inside the denitrator. Magnesium nitrate concentration in the feed was kept 150 g / l for five runs and later was increased to 325 g / l for 4 runs. Feed rate was kept around 6 lph and temperature inside the column was maintained in the range of 425 - 450°C for all the runs.

In these runs conversion in the range of 95 to 98% was achieved. However both global agglomeration inside the bed and local caking around the spray nozzle were observed. Operation could not be carried out for long duration and the run had to be terminated mainly because of either defluidization of the bed due to agglomeration or heater failure.
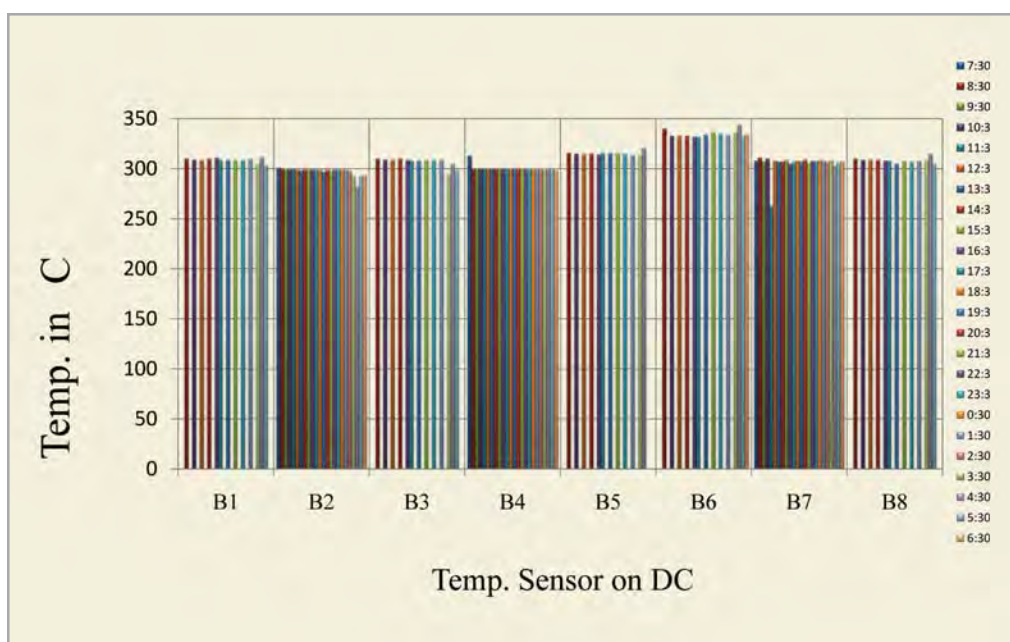
Fig. 2: A typical temperature profile inside the denitration column. B is bed temperature at different axial locations.

Considering the above for further operation, following two major changes were made in the plant before carrying out second phase of runs:

1. Electric resistance heater was replaced by induction heater.

2. Upward facing spray nozzle placed in the column was used for feeding.

With these changes six runs were taken in the second phase of plant operation. Feed concentration in all the six runs was fixed at 285 g / l of magnesium nitrate. Feed rate and column temperature were maintained in the same range as in the first phase. Induction heater was established as a robust source of heat. With change in feed nozzle orientation, problem of local caking around the nozzle could be overcome. However the problem of global agglomeration still existed and needs to be solved by further experimental work. In these runs also, high conversion, in the range of 95 – 98 % was achieved.

Experience with Ammonium Nitrate Solution

Uranyl nitrate solution obtained from refining

process is precipitated as Ammonium Di-uranate (ADU). After removal of the precipitate, filtrate generated contains mainly ammonium nitrate solution. Process feasibility studies for thermal denitration of ADU filtrate were carried using synthetic ammonium nitrate solution.

Experimental runs were carried out at two concentration levels in the feed: 75 g/l and 150 g/l and at a feed rate of 6 lph. Operating temperature was kept between 300- 350°C. Smooth steady state plant operation for extended duration could be established. A maximum operating period of 90 hrs could be achieved with 75 g/l of ammonium nitrate solution. Conversion levels obtained in these runs varied between 50-70 %. Unconverted ammonium nitrate can be selectively separated from the off gas and recycled back for denitration.

Experience with Zirconium raffinate solution

Raffinate stream generated in Zirconium refining process carried out in NFC, Hyderabad was also treated in the facility. The composition of the raffinate stream received from NFC is given in Table 1 and the decomposition temperature of

Table 1: Composition of the raffinate stream received from NFC

Component	ChED lab Analysis	NFC Analysis
Free Acid	3 N	2.0-4.0 N
ZrO_2	3.8 gpl	< 3.0 gpl
Hf ratio	-	20-40%
Na	9050 ppm	-
Fe	734 ppm	-
Si	154 ppm	-

various nitrates present in the stream are given in Table 2.

Operation was carried out at a temperature of 400° C and bed got defluidized due to agglomeration inside. Experiments were repeated at a temperature of 200° C and similar problem was observed. However this was not observed with synthetic feed solution prepared. Chemical analysis of the raffinate solution was carried out by Chemical Engineering laboratory and it was found that low melting nitrates like ferric nitrate and sodium nitrate are present leading to agglomeration inside the bed. Sulphuric acid was added to the feed to take care of ferric nitrate and operation was repeated at 200° C. Smooth operation was achieved and ~70% nitric acid could be recovered at a concentration of 3 N. Zr raffinate has high nitrate content which cannot be disposed off and thermal denitration is a potential treatment process for the stream.

Pilot Plant

A pilot plant has been set up to study the denitration process at higher capacity. The plant has 300 NB denitration column and has been designed for a capacity of 30 lph of feed. The plant uses twin feed nozzle system i.e. two nozzles can be used at a time for feeding. Each nozzle has a stand-by that can be put on line if the active one gets choked. Two induction heaters axially divided over the length of the column have been used. The two heaters are controlled independently using PID controllers. Fig. 3 shows Denitration column with induction heater coils.

Ammonium nitrate retrieval vessels have been used in the plant for recovery of unconverted ammonium nitrate.

The plant has been commissioned with water as feed from two spray nozzles at a rate of 42 lph. Uniform temperature profile was obtained inside the column with two induction heaters and continuous solid circulation was achieved.

Trial run was taken with ammonium nitrate solution in the plant. The run was divided into 3 sub-parts:

1. Operation with single feed nozzle with flow rate of 15 lph

Table 2: Decomposition temperature of various nitrates present in the stream

Component	Melting point C	Boiling point C	Decomposition point C (Extent of decomposition)
Pure Zirconium nitrate	-	-	320 (90%) 600 (100%)
Nitric acid solution	-	120	200 (66%)
Sodium nitrate	308	-	700 -900
Ferric nitrate	35	-	-
Ferric sulphate	480	-	-

Fig. 3: 300 NB Denitration Column with induction heater coils

2. Operation with two nozzles with total flow rate of 30 lph.

3. Operation with two nozzles with total flow rate of 42 lph.

Continuous stable operation was established and data has been collected for determining conversion. A typical temperature profile obtained at 42 lph feed rate is shown in Fig. 4.

The plant can be used for thermal denitration of uranyl nitrate. Once established, direct denitration technology of Uranyl nitrate would eliminate multi-step operation involved in Ammonium Di-Uranate (ADU) route and mitigate nitrate effluent disposal difficulties. In trials with magnesium nitrate on bench scale, conversion in the range 95 to 98% has been achieved on bench scale. However, with prolonged operation, global agglomeration inside the bed was observed, which results in de-fluidization. To overcome this, studies on in-bed agglomeration and particle break down dynamics have been planned
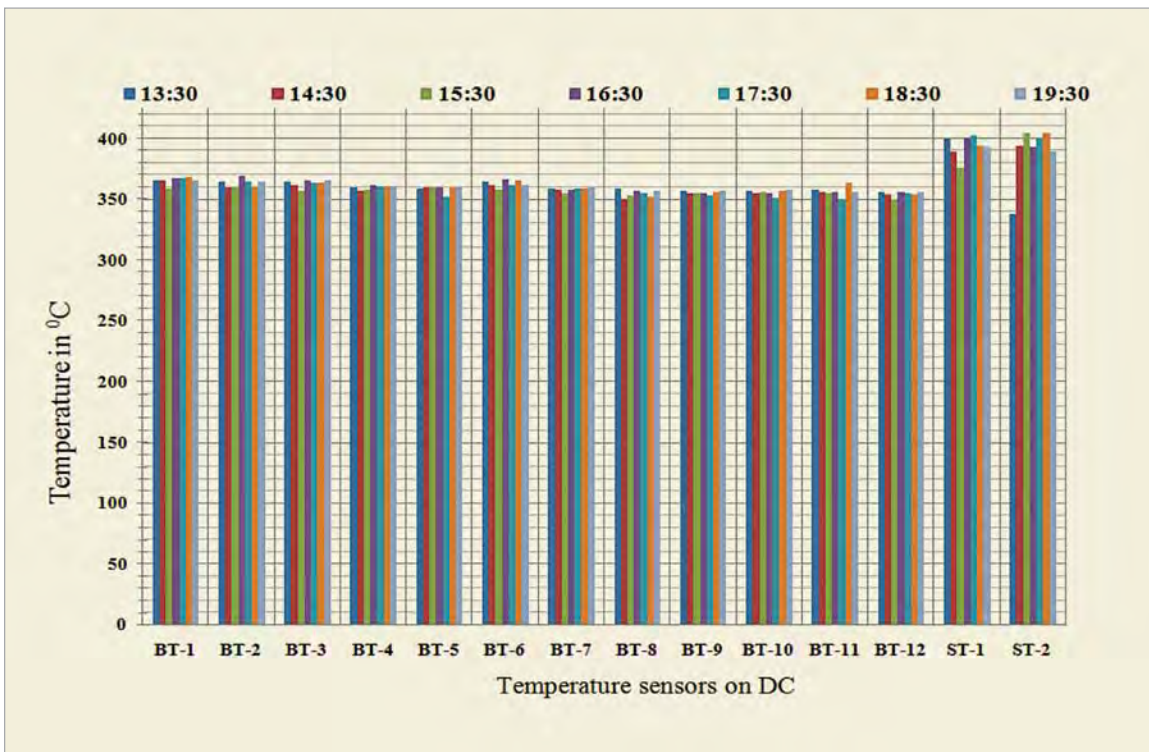

Fig. 4: Temperature Profile inside Denitration Column with 42 lph of ammonium nitrate feed. B is bed temperature at different axial locations, S is wall surface temperature

in the pilot scale facility. This will include study of jet grinders and optimization of operating and design parameters to overcome the problem of agglomeration.

Experience with Ammonium Nitrate Solution

Parametric studies were carried out in the 300 NB denitration column with synthetic ammonium nitrate solution for optimization of operating conditions. Effect of feed flow rate, temperature, fluidization air flow rate and nozzle orientation on conversion has been studied. Feed concentration of 130 g / lit was kept constant in all the runs.

Feed can be introduced inside the reactor through single or two nozzles at a time. It is observed that splitting of feed through two nozzles gives higher conversion. Also increase in conversion is observed with increase in temperature from 300° C to 350° C. Operation at 370° C gave further increase in conversion. Nozzle orientation was kept upward in first 6 runs and later other column was used with feed nozzles placed horizontally. There is not any effect observed on the conversion with the change in orientation of nozzles. Fluidization air flow rate has some effect on wall heat transfer coefficient. However it does not seem to have much effect on nitrate conversion. Operations with feed flow rates 20 LPH, 30 LPH and 40 LPH show that there is decrease in conversion with the increase in feed flow rate. Decrease in ALR (Air to Liquid ratio) also favours higher conversion.

Table 3: Summarizes the data obtained in the pilot plant study

Parameter	Temperature C	No. of Feed Nozzles and orientation	Feed flow rate LPH	ALR Slpm of air / lpm of feed	Fluidization Air flow Rates lpm	Conversion %
RUN 1	300	1 , 45° upwards	20	830	800	42
RUN 2	300	1 , 45° upwards	15	830	800	54
RUN 3	300	1 , 45° upwards	15	780	800	57
RUN 4	350	1 , 45° upwards	15	830	800	62
RUN 5	350	2, 45° upwards	20	780	800	61
RUN 6	350	2, 45° upwards	30	780	800	48
RUN 7	350	2, 45° upwards	40	780	800	38
RUN 8	350	2, horizontal	30	780	800	48
RUN 9	350	2, horizontal	30	780	600	49
RUN 10	370	2, horizontal	30	780	800	56

It is observed that conversion of ammonium nitrate is much lower as compared to magnesium nitrate. In case of magnesium nitrate the reaction takes place in the emulsion phase on the surface of the silica particles, resulting in almost complete conversion due to high residence time in the emulsion phase. Ammonium nitrate decomposition is a vapour phase reaction and takes place both in emulsion and bubble phases. Because of very low residence time of ammonium nitrate in the bubble phase conversion is low compared to magnesium nitrate. However the unconverted Ammonium nitrate can be recovered from the off-gas and recycled.

Denitration plant in Uranium Oxide Facility (Kalpakkam)

Till the technology of direct denitration of uranyl nitrate is established and deployed, conversion of uranyl nitrate to oxide would be through Ammonium Di-Uranate (ADU) precipitation route with generation of ADU filtrate containing ammonium nitrate. Process feasibility has been established for thermal denitration of ADU filtrate on the bench scale facility starting with synthetic ammonium nitrate solution. Ammonium nitrate being explosive in nature, a detailed process calculation was carried out to arrive at safe range of operating conditions inside the denitration column. Information and design data collected and technology developed on bench and pilot scales is being deployed for treating ADU filtrate

generated from Uranium Oxide Facility (UOF), Kalpakkam. In case the situation demands, this can be deployed for overcoming the problem of disposal of ADU filtrate stream generated at the front end.

Conclusion

Fluidized Bed Thermal Denitration Technology has been developed and is being deployed for ADU filtrate at UOF (Kalpakkam). The technology has potential for treating various nitrate streams viz. Uranyl nitrate, Zirconium raffinate and it involves stream specific development. Nitrate waste from both front & back end of nuclear fuel cycle can be disposed with minimum environmental impact by Fluidized Bed Thermal Denitration Technology.

Acknowledgements

MetProSoft-10: Image Analysis Software for Metallographic Measurements

Lizy Pious, S. Kar and V.M. Joshi

Electronics & Instrumentation Services Division

Summary

MetProSoft-10 package provides a number of features which are important for material characterization by performing metallographic measurements on images. Developed in VC++ under Windows XP, the package is user friendly. However, the software can be enhanced further by incorporating features which includes compatibility to different image file formats, report generation, measurements as per ASTM standards, acquisition from input devices and display of user specified overlay patterns on images to facilitate measurements.

Introduction

Image processing and analysis techniques find extensive applications in metallographic measurements and analyses. EISD (BARC) has been engaged in this development and by virtue of sustained efforts over last several years, a very comprehensive package named MetProSoft-10, consisting of various image processing and analysis utilities have been developed. The technology of MetProSoft-10 has been transferred to M/s QS Metrology Pvt. Ltd, New Delhi for enabling wide usage in industry and elsewhere.

With the help of MetProSoft-10, the user can process 8 bit monochrome images of varying spatial resolutions that may be acquired from image acquisition devices like digital cameras, analog cameras connected to PC based frame grabbers, scanners etc. This package is a collection of software based processing and analysis tools that enable the user to perform various measurements on images displayed from BMP format grey level image files. This Graphical User Interface (GUI) based software is user friendly and operates in an interactive manner.

The main functionalities of MetProSoft-10 include image display, histogram computation and plot display, segmentation by histogram-based interactive thresholding, interactive spatial calibration, geometric measurements, phase measurement, feature counting and grain size estimation. This paper provides details regarding salient features that enable the user to carry out the desired operations on images for obtaining the results or data of interest. Major functions available in this package are described below with the help of illustrative images.

Functional Description

- MetProSoft-10 provides the user with menu driven commands to display an image, perform spatial calibration using known reference and add calibration marker to the image. The user can also set a Region of Interest (ROI) on the image interactively, copy that part of the image, paste it as a new image and proceed with the measurements tools. The image title, image size, image resolution, the cursor position, grey level of the image at the cursor position and size of the ROI are displayed on the application window.

- The program provides Geometric measurement tools including line, angle, rectangle and circle that can be dragged, dropped and resized on the image window. In addition, 2-point line, 3-point circle and polygon tools are provided which are drawn interactively by the user.

Fig. 1: Angle Tool
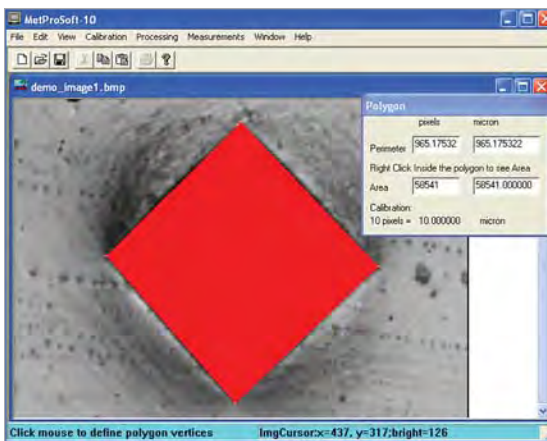
Fig. 2: Polygon Tool

- MetProSoft-10 has capability to display histogram of the displayed image on a scrollable and resizable window. On the histogram window, user is provided with a cursor that can be dragged and dropped along the grey level axis of the plot. At any position of the histogram cursor, the grey level as well as the count of occurrence of the grey level on the image are displayed on the status bar of the application window.

- MetSoft-10 facilitates image segmentation by histogram based interactive thresholding. While this tool is enabled, the histogram window displays a threshold window with two cursors that represent the lower and upper grey level threshold values. Both the cursors can be
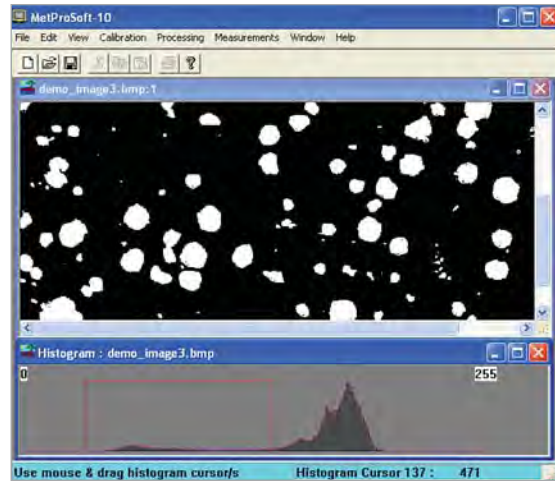
Fig. 3: Interactive Thresholding

independently positioned along the grey level axis to set a threshold window. The result of image segmentation is a binary image with only black and white levels (as shown in Fig. 3), which can be saved by the user as a BMP file.

- The phase measurements tool provided in the program has the option to choose the number of phases to be displayed and measured, as shown in Fig. 4. The selected phases can be displayed in different colors on the image window and histogram plot appears with cursors for selecting upper and lower threshold values of the phases. The image window displays the updated phases as the thresholds are updated by the user. The grey level and frequency at the selected cursor position on
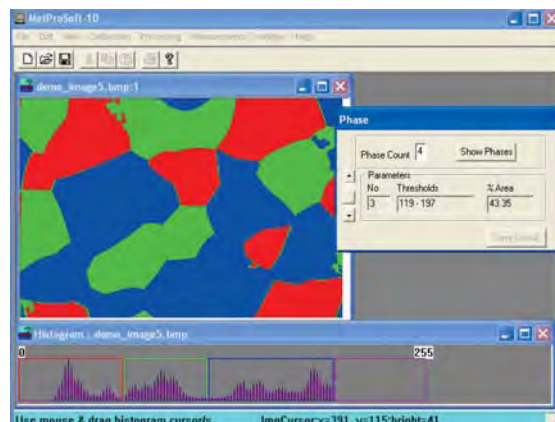
Fig. 4: Phase Measurements
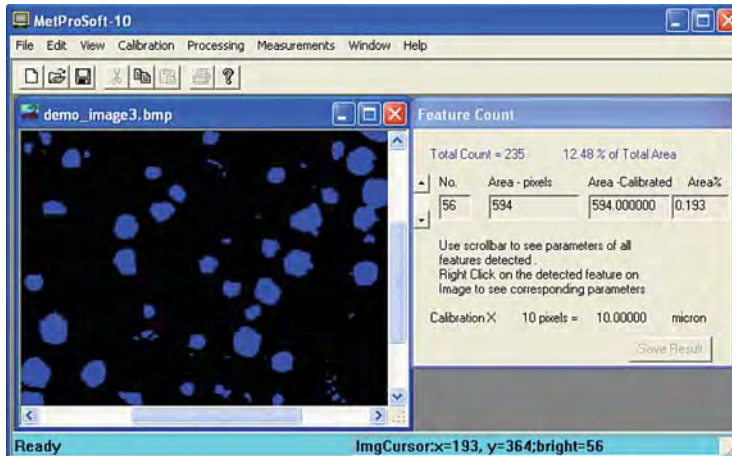
Fig. 5: Feature Counting
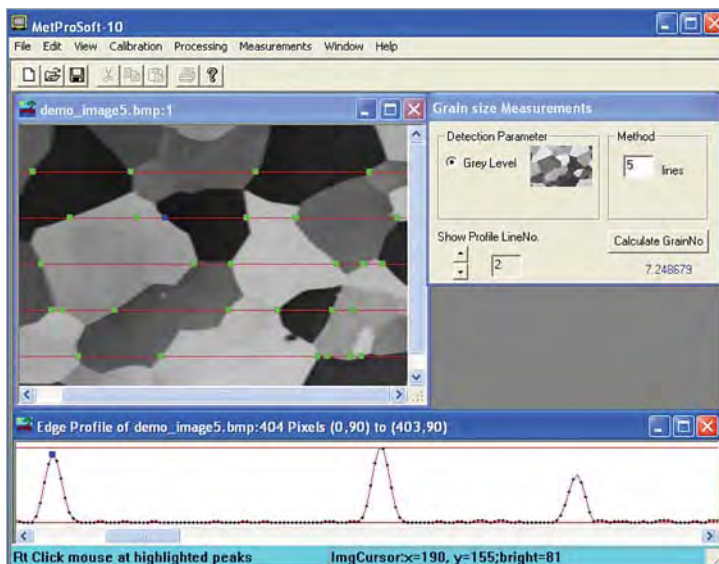
Fig. 6: Grain Number Measurement

the histogram window are displayed on the status bar. User has the option to scroll through and view the calculated parameters of the selected phases as well as save the parameter list as a text file.

• The feature counting tool provided in MetSoft-10 detects features that have grey level values between automatically calculated lower threshold and maximum grey level (white). Typical application window for this option can be seen in Fig. 5. The image window displays the detected features in blue color and

a dialog box appears showing the count and percentage area of features detected. User can select any feature on the image and view the corresponding parameters. Alternatively, user has the provision to scroll through the feature parameter list which can be saved as a text file.

• MetProSoft-10 provides a Grain Size tool that calculates the grain number based on horizontal line intercepts at the edges of grains. The line profiles of the image with detected peaks highlighted are displayed on a separate window. The number of line profiles to be selected is user selectable. GUI is provided to select the line profile to be plotted on the profile window and verify the correspondence between peaks on edge profile and edge on the image window. Some details of this operation can be inferred from Fig. 6.

Acknowledgement

References

1. Digital Image Processing by Rafael .C. Gonzalez and Richard E. Woods, Pearson Education, Inc., 2002.

2. Digital image processing algorithms and applications by Ioannis Pitas, John Wiley & Sons, Inc., 2000.

Passive Gamma Scanning : a Powerful Tool for QC of MOX Fuels

K.V. Vrinda devi and J.P. Panakkal
Advanced Fuel Fabrication Facility
Nuclear Fuels Group
Bhabha Atomic Research Centre, Tarapur

Abstract

Passive gamma scanning (PGS) had been used in nuclear fuel industry for various applications such as characterization and assay of nuclear waste, enrichment monitoring of nuclear fuel pins and post irradiation examination of irradiated fuel. (U,Pu)O$_2$ mixed oxide (MOX) fuels have been developed in India for irradiation in thermal and fast reactors. MOX fuels for various reactors have been fabricated at Advanced Fuel fabrication facility (AFFF), BARC, Tarapur. PGS technique was modified and studies were carried out on these fuels to extract detailed information regarding the composition and configuration of a wide variety of MOX fuels.

Introduction

MOX fuels are fabricated through the powder metallurgical route starting from mixing of UO$_2$ and PuO$_2$ powders, granulation, compaction and sintering. Sintered pellets are encapsulated in Helium filled clad tubes and welded with end plugs [1].

Use of passive gamma scanning (PGS) has been reported for checking the enrichment and its uniformity in enriched UO$_2$ fuels [2]. Monitoring of Pu content in MOX fuel pins was tried with PGS, but high accuracy could not be attained due to low count rates [3]. Currently, PGS is being employed as a quality control inspection for enriched UO$_2$ fuel pins for TAPS fabricated at Nuclear Fuel Complex (NFC), Hyderabad and (U,Pu)Mixed Carbide fuel(MC) pins for FBTR fabricated at Radiometallurgy Division (RMD),BARC,Mumbai for enrichment check. Studies have been carried out with PGS at AFFF, BARC, Tarapur to extract detailed and accurate information regarding the composition, homogeneity and configuration of the MOX fuel stack covering a wide range of composition and configuration.

Gamma scanner at AFFF

The fuel pin scanner at AFFF with a fuel pin input and output magazines of 4m length each was originally designed for BWR fuel pins [Fig.1]. A 3" X 3" NaI(Tl) detector was used for the assay and a segmental scan was carried out. The detector was collimated using 25mm thick Tungsten-Nickel-Copper alloy with slit width 12mm to virtually divide the pin into a series of equally wide segments. The slit size and scanning speed were optimized so that each pellet (nominal length of 14mm) was assayed inside a welded BWR fuel pin to acquire a good count rate. Although the technique was effective in detecting cross mixing of enrichments, the accuracy of estimation of average PuO$_2$% of the pin was only ±0.2 %(abs.) [4].

Fig. 1: Gamma Scanner at Advanced Fuel Fabrication Facility, BARC, Tarapur loaded with a BWR fuel pin
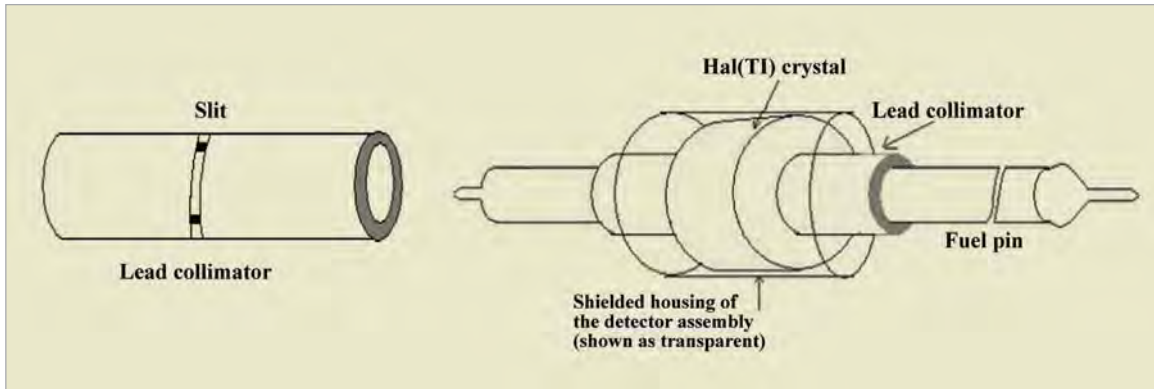
Fig. 2: Counting geometry with annular shaped detector and collimator

Annular shaped NaI(Tl) detector

An annular shaped NaI(Tl) detector with a pipe shaped Lead collimator was introduced for improving the counting geometry. The through well geometry provided a complete circumferential coverage to the source increasing the count rate drastically. Error in counting could be reduced to 1% with a reduced slit width and increased speed of scanning (10mm/sec). This further caused an improvement in the spatial resolution as well as in the accuracy of estimation of PuO_2% of the source. The detailed counting geometry of the annular detector assembly is shown in Fig.2.

A comparative study was carried out with both the detectors using BWR MOX fuel pins and the results are presented below.

MOX fuel for Thermal Reactors

Experimental MOX fuel assemblies have been irradiated in thermal reactors in India. MOX fuels loaded in thermal reactors are of low PuO_2 content varying from 0.4% to 3.25%.

MOX fuel pins for BWR

(U,Pu) MOX fuel was considered to be a viable alternative to the imported enriched UO_2 fuel. The fuel pins were of three different PuO_2% namely 0.9%, 1.55% and 3.25%. Gamma scanning studies conducted on these fuel pins showed a linear correlation between PuO_2% and count rates.

The correlations between the average PuO_2% of the pin and the average count rate were as shown below. The correlations were fitted by the method of least squares with a correlation coefficient better than 0.99.

$$\text{Count rate} = (1295*PuO_2\%) + 42.96 \qquad (1)$$
[conventional detector]

$$\text{Count rate} = (2099*PuO_2\%) + 2107 \qquad (2)$$
[annular detector]

From this correlation, Passive gamma scanning using annular detector set up was found to be capable of estimating the average PuO_2% of the fuel pin with an accuracy of ±0.1% (abs.) and a confidence of 95% (2σ). The sensitivity of the system increased by 100%, thereby, improving the accuracy of estimation ±0.1% (abs.) as compared to ±0.2% (abs.) in the conventional set up. Fig.3 shows a comparison of calibration graphs of both the detectors [5].
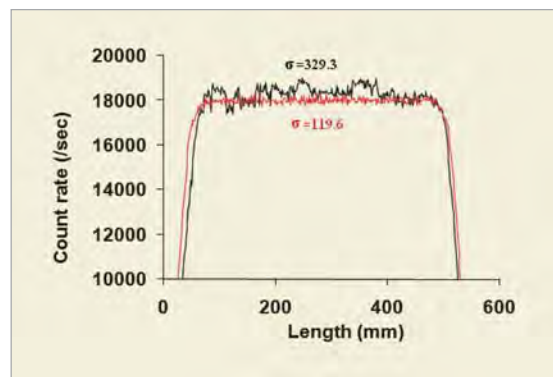
Fig. 3: PuO_2% Vs. Count rate – Comparison of two counting geometries

MOX fuel pins for PHWR

PHWR MOX fuel subassembly consisted of 7 MOX fuel pins with 0.4% PuO_2 surrounded by 12 natural UO_2 pins (MOX-7 design).

The PuO_2 content of the MOX fuel was specified to be $0.4 \pm 0.1\%$(abs.). It was also specified that the average PuO_2 content of the central pin should not be less than 0.03%(abs.) than the surrounding 6 pins. Hence it was necessary to estimate the average PuO_2 content with accuracy better than $\pm 0.1\%$(abs.).

Due to the through well counting geometry, the relative error also decreased from 3.9% (with conventional counting geometry) to 1.6% for this composition and hence, the estimations could be done with better accuracy and precision.

PGS was found to be effective in PHWR MOX fuel pins for :- [6]

- Estimating the average PuO_2 content of every fuel pin with accuracy of $\pm 0.02\%$ (abs.) so that the pins could be screened for the central position.

- Detecting variation of PuO_2 content within a fuel stack by more than 0.03% if the deviant portion is atleast of length 15cm

- Gamma scan of a pin which contained pellets from two batches with deviance in PuO_2% by 0.02% is shown in Fig.4.

MOX fuel for Fast reactors

Fuel pellets for fast reactors are of small diameter
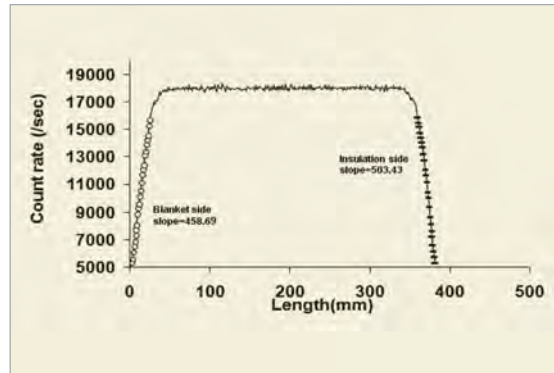
Fig.4: Gamma scan of a PHWR MOX pin with variation in PuO_2 content in the stack

and are annular in shape. So, effectively the thickness of the pellet to be probed was less in fast reactor fuel pellets. FBTR MOX fuel pins contain annular geometry fuel pellets of 5.52 ± 0.04 mm outer diameter and 1.8 mm (nominal) internal diameter. The effects of self shielding offered by FBTR MOX pellet and the probing depth of the technique was calculated and it was found that the penetration depth of 400keV gamma rays in MOX fuels for FBTR and PFBR ranged from 1.9-2mm [7].

MOX fuel pins for FBTR

Fuel pin for a few MOX subassemblies were fabricated at AFFF for the hybrid core of FBTR and irradiated in the reactor. PuO_2 content of these fuel pins were specified to be $44\pm 1\%$(abs.). The schematic diagram of the FBTR MOX fuel pin is shown in Fig.5.

PGS could be used during FBTR MOX fuel fabrication for

- Estimation of average PuO_2 percentage in
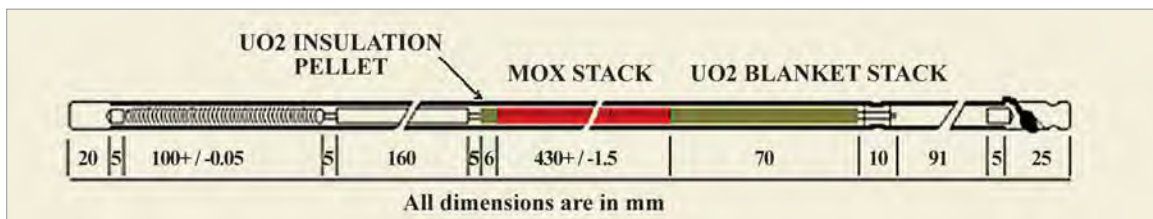
Fig. 5: Schematic drawing of FBTR MOX fuel pin

a fuel pin with an accuracy of ± 0.6 % (abs.) and detecting heterogeneity in PuO_2 distribution beyond 1.5% (abs.).

- Ensuring correct sequence of loading of blanket, insulation and fuel pellets and no cross mixing of blanket pellets with fuel pellets and

- Detecting Pu rich agglomerates located anywhere in the fuel which is richer by 0.6% (abs.) or more and estimating the minimum richness of any detected agglomerate.

The passive gamma scans of two pins with large difference in σ value are shown below in Fig.6. Variation of σ from the theoretically estimated value indicated Pu heterogeneity.

It was possible to distinguish the blanket/insulation
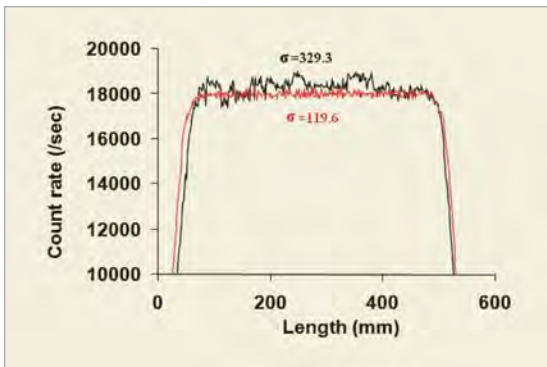
Fig. 6: Gamma scan indicating inhomogeneous distribution of PuO_2 in the fuel
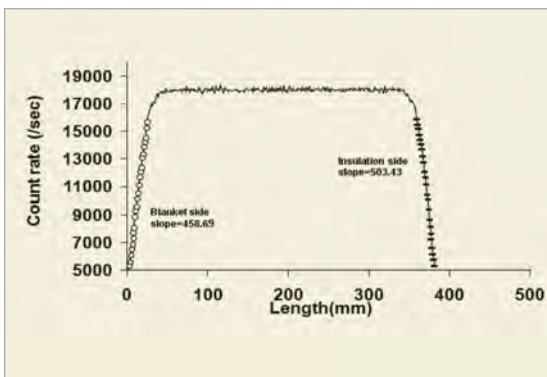
Fig. 7: Gamma scan of FBTR MOX fuel pin showing different slopes at Blanket pellets side   and Insulation pellet

pellets (see Fig.6) from the slope of rising/trailing ends of the gamma scan as shown in Fig.7.

MOX fuel for PFBR

Fuel pins for PFBR are approximately 2.6m long with a 1000mm long MOX stack and 300mm long axial blanket (UO_2) on either side [8].   The composition of the fuel is 21wt% PuO_2- UO_2 (for the inner core region) and 28 wt% PuO_2-UO_2 (for the outer core region). Fuel for the initial core of PFBR is being currently fabricated at AFFF, BARC, Tarapur. PGS was used during the fuel fabrication for the following detections [9].

- Estimation of average PuO_2 percentage in a fuel pin with an accuracy of ± 0.1%(abs.) with 3σ confidence.

- Detecting 100% PuO_2 agglomerates of large size (more than 1mm) located anywhere in the fuel and of size 550 μm or more located near the outer surface.

- Estimating the minimum richness and diameter of any detected agglomerate

- Ensuring correct sequence of loading of blanket and fuel pellets

Gamma scans of two PFBR pins with a variation of 0.15% in PuO_2 content are shown in Fig.8 and scan of a pin with cross mixed fuel and blanket pellets is shown in Fig. 9.
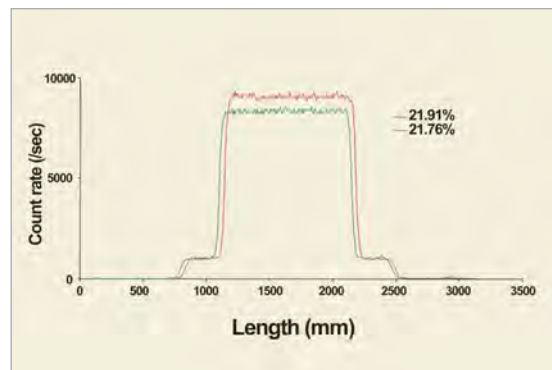
Fig.8: Gamma Scans of PFBR pins with varying average PuO_2 content
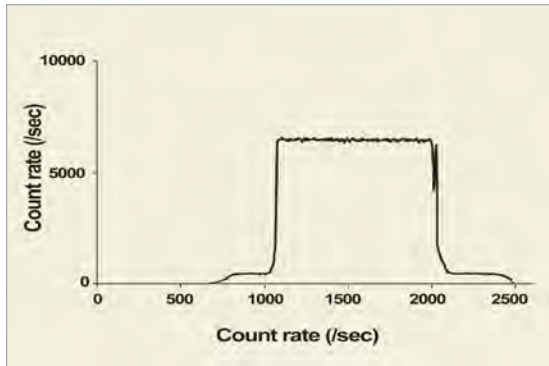
Fig. 9: Detection of a blanket pellet in MOX fuel stack in a PFBR fuel pin
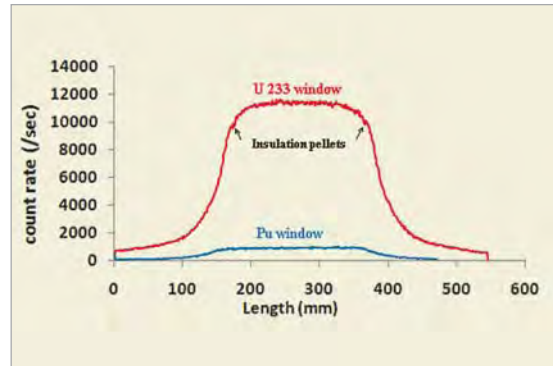
Fig.10: Gamma scan of a typical experimental fuel pin in dual window

U²³³ bearing (U,Pu) MOX fuel pins

A test subassembly simulating the fuel for PFBR was loaded in the Fast Breeder Test Reactor (FBTR) for irradiation. The composition of the fuel was $(0.71U-0.29Pu) O_2$ with 53.5% enrichment in UO_2 with $U^{233}O_2$. This unique composition is designed to simulate the thermo-mechanical conditions of the fuel composition of PFBR in FBTR. PGS was employed for monitoring the composition of the fuel both in terms of $U^{233}O_2$ and PuO_2. The counting window of 300-450 keV was used for the purpose of assaying the pin for its Plutonium content. The counting window was set to count gamma rays of energy from 600keV to 1.6 MeV for assaying U^{233}. Conventional 3"x 3" detector was used for counting as the count rates were very high.

A number of calibration pins were fabricated for the gamma scanning studies. Care was taken to use only one lot of PuO_2 and $U^{233}O_2$ powder while fabricating the calibration pins. PGS could be used in U^{233} bearing fuel [10]:-

- to monitor the variation of average $U^{233}O_2$ content beyond ±1%.

- to monitor the variation of average PuO_2 content beyond ±1% and

- to confirm the correct loading of insulation and fuel pellet

Passive gamma scans acquired through dual window,
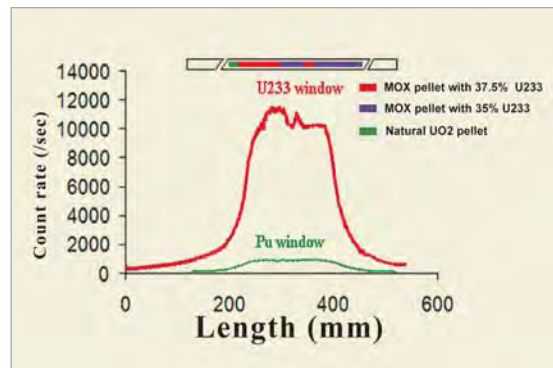
Fig.11: Dual window gamma scans and the schematic drawing of the calibration pin

of a typical experimental MOX fuel pin and a calibration pin are shown in Figs.10 &11. The scans were carried out both in Pu and U^{233}window individually.

Conclusion

Passive Gamma scanning with improved counting geometry has been carried out on (U,Pu) MOX fuels with a wide range of composition and configuration. The technique has been found to be capable of extracting detailed compositional information of MOX fuel pins such as average PuO_2 content, homogeneity of PuO_2 in UO_2 matrix, loading configuration of fuel and blanket pellets etc. It was possible to detect Pu rich agglomerates in MOX fuel and also estimate its size. It could also be used for independently estimating the variation in $U^{233}O_2$ and PuO_2 in fuel pins containing both. The technique being non destructive could be applied

to all the fuel pins as opposed to the destructive techniques carried out on random samples. PGS is a prompt technique and hence suitable technique for fuel fabrication facilities with high throughput. It reduces load on conventional chemical analysis and hence could considerably reduce the generation of radioactive liquid waste. Since it reduces load on autoradiography techniques, radioactive exposure to personnel could also be significantly reduced.

Acknowledgement

References

1. H.S.Kamth, S.Majumdar, DSC Purushotham, Development in MOX pellet fabrication technology- Indian Experience, IAEA- TECDOC no.1036 , 1996.

2. J.P. Panakkal, Proced. of International Symposium on Advanced Nuclear Materials, Mumbai, 2006.

3. P. Mainy, C.Morin. Fuel rod enrichment determination by gamma scanning. *Journal of Nuclear Materials* Vol 178,1991, 261-265.

4. T. Soreng, K.V. Vrinda devi, J.P. Panakkal, H.S. Kamath, Passive Gamma Scanning for non-destructive characterisation of mixed (MOX) fuel pins for BWR, *Insight* Vol 47 No.9 Sept.2005, 536 – 537.

5. K.V. Vrinda devi, T. Soreng, J.P. Panakkal, H.S.Kamath, Use of Annular Scintillation detector for Passive Gamma scanning of BWR MOX Fuel pins, Proceeding of the International conference Characterisation and Quality Control of Nuclear Fuels, India, 2002 , 599-603.

6. K.V. Vrinda devi, T. Soreng, J.P. Panakkal, H.S.Kamath, *Nuclear Technology* Nov.2008 Vol 164 No.2, 305-308.

7. J.P. Panakkal, K.V. Vrinda devi, T. Soreng, Proced. of International conference on Advanced Nuclear Materials, Mumbai, 2011.

8. S.C. Chetal, V. Balasubramanian, P. Chellapandi, P. Mohanakrishnana, P. Puthiyavinayagam, C.P. Pillai, S. Raghupathy, T.K. Shanmugham, C . Sivathanu Pillai, *Nuclear Design and Engineering* Vol. 236(7-8) April 2006, 852-860.

9. K.V. Vrinda devi, T. Soreng, D. Mukherjee, J.P. Panakkal , H.S. Kamath; *Journal of Nuclear Materials* 399 (2010), 122-127.

10. K.V. Vrinda devi, T. Soreng, J.P. Panakkal, H.S.Kamath; *Nuclear Design and Engineering* 241 (2011), 2783-2786.

Technology Transfer Know-Hows from BARC: a report

"Dip N Drink membrane pouch" technology

The technology of "Dip N Drink membrane pouch" has been developed by the Desalination Division, BARC. The Membrane Pouch is based on Osmosis process to get sterile drinkable solution from biologically contaminated water, especially during disaster conditions like flood, cyclones, tsunami, earthquakes and the useful for concentration of high value low volume product in food, pharmaceutical, chemical industries. It can also be used in Oral Rehydration Therapy in remote areas and villages.

The know-how of "Dip N Drink membrane pouch" was transferred to M/s Aum Technologies, Kharghar, Navi Mumbai on December 26th, 2011.

Photograph after signing the agreement with M/s Aum Technologies, Kharghar, Navi Mumbai (Maharashtra), seen from left to right Shri V. K. Upadhyay, TT&CD, Shri B. K. Pathak, Head, IPMS, TT&CD, Shri S. G. Markandeya, Head, TT&CD, Shri Neeraj Bhandari, Partner, M/s Aum Technologies, Shri Pankaj Bhandari, Partner, M/s Aum Technologies, Dr. P. K. Teewari, Head, DD, Dr. S. Prabhakar, Head, STS, DD, Dr. R. C. Bindal, DD, & Dr. A. K. Ghosh, DD.

"Glass to Metal Seals" technology

The technology of "Glass to Metal Seals" has been developed by the Glass & Advanced Ceramics Division, BARC. Glass to metal seals are vacuum tight assemblies, in which metallic wires, tubes, eyelets or flanges are firmly bound in a glass material. These are normally used as insulated feed-through for electrical connections in hermetically sealed devices and UHV systems as well as mounts for electrodes, filaments etc. The materials chosen have the properties of wettability by glass, matched temperature coefficients of expansion and low outgassing rates even at elevated temperatures making them suitable for application in ultra high vacuum systems. This technology has been

developed for various types of glass to metal seals- like flat bead seals, circular bead seals, eyelet type seals, tubular seals, wafer base seals and glass to metal feedthroughs for high pressure applications.

All these types of seals are being produced in BARC. and are being used in several in-house applications

in the Department of Atomic Energy and its research centres.

The know-how was transferred to M/s Span Manufacturing Co. Pvt. Ltd., New Delhi on February 21st, 2012.

Photograph after signing the agreement with M/s Span Manufacturing Co. Pvt. Ltd., New Delhi seen from left to right Shri H.Y. Bodari, GACD, Radhakrishnam S. Nair, GACD, Shri Yogesh B. Shirkar, GACD, Shri Ramesh G. Barge, GACD, Dr. G.P. Kothiyal, Head, GACD, Ms. Surbhi Jindal, GM, M/s Span Manufacturing Co. Pvt. Ltd., New Delhi, Shri Neeraj Jindal, MD, M/s Span Manufacturing Co. Pvt. Ltd., New Delhi, Shri S. G. Markandeya, Head, TT&CD, Shri B. K. Pathak, Head, IPMS, TT&CD & Shri V. K. Upadhyay, TT&CD.

2nd Theme meeting on Very High Energy Gamma-Ray Astronomy: a report

The 2nd theme meeting on Very High Energy Gamma-Ray Astronomy was organized by the Astrophysical Sciences Division during March 29 - 31, 2012 at the Mt. Abu based Gamma-Ray Observatory. 41 delegates from Tata Institute of Fundamental Research, Mumbai, Physical Research Laboratory, Ahmedabad, Saha Institute of Nuclear Physics, Kolkata, Aryabhatta Research Institute for Observational Sciences, Nainital, Guwahati University, Dibrugarh University and Bhabha Atomic Research Centre participated. The meeting comprised of 12 invited talks and 25 contributed presentations.

The theme meeting was inaugurated by Dr. S. Kailas, Director, Physics Group, BARC who emphasized the need for collaborative work in the emerging field of ground based gamma-ray astronomy. The recent results obtained by the TACTIC and HAGAR telescopes were discussed in detail. A separate session was devoted to the proposed Cherenkov Telescope Array project and the modalities of Indian participation in this international project were discussed. The theme meeting was fully funded by the Board of Research in Nuclear Sciences.

Participants of the Theme Meeting with Dr. Kailas, Director, Physics Group, BARC

Microwave based Denitration of Heavy Metal Nitrate Solution: an MoU with SAMEER

BARC has entered into collaboration with the Society for Applied Microwave Electronics Engineering and Research (SAMEER), Mumbai for developing microwave heating system for denitration of Heavy Metal Nitrate solution. SAMEER is an autonomous R&D institute of Department of Electronics & Information Technology (DeitY), Ministry of Communication and Information Technology, Govt. of India.

Shri S. D. Misra, Director, Nuclear Recycle Group, BARC and Dr. A. L. Das, Director, SAMEER signed memorandum of understanding (MoU) for collaboration towards development of microwave heating system in Trombay on 1st June 2012.

SAMEER has the expertise in area of RF and microwave engineering and has interest in joint technology development projects. Nuclear Recycle Group, BARC requires a simple and efficient method for direct denitration of heavy metal nitrate solution. This collaboration is expected to develop a microwave heating system which enables to carry out basic R&D for denitration of heavy metal nitrate solution. Fuel Reprocessing Division, NRG will utilise the system to establish various parameters to carry out microwave denitration of heavy metal nitrate solution.

From Right to Left: Shri S S Prasadh, Shri P. M. Gandhi, (Head, FRD) Shri A. L. Das (Director, SAMEER) Shri S. D. Misra (Director, NRG) Shri Rajesh Harsh, Shri Y. C. Shivkumar, Shri R. Bansal, Shri G. Sreekumar.

A Report on
ISEAC International Symposium cum Workshop on Electrochemistry (ISEAC-WS-2011)

ISEAC International Symposium cum Workshop on Electrochemistry (ISEAC-WS-2011) was organized by Fuel Chemistry Division of RC&I Group, BARC at Goa during December 7-10, 2011 to celebrate the International Year of Chemistry (IYC-2011). The Indian Society for ElectroAnalytical Chemistry (ISEAC) provided this platform to commemorate the achievements in electrochemistry, to explore the challenges to be taken up and to motivate young research scholars.

The inauguration function was held in the evening of December 6, 2011. Prof. S.K. Aggarwal, President, ISEAC, Chairman, Organising Committee welcomed all the delegates of ISEAC-WS-2011 and briefed about the activities of ISEAC since its inception in October,

2003. Shri Saurav K. Guin, Secretary, ISEAC, Convener, Organising Committee presented a summary about the various topics of both fundamental and applied Electrochemistry to be discussed during ISEAC-WS-2011. Dr. (Mrs.) J.V. Kamat, Treasurer, ISEAC, Co-Convener, Organising Committee, proposed a vote of thanks.

About 100 participants including 6 overseas speakers participated in the event. There were 16 Invited talks, 2 Short Lectures, 21 Contributed Papers and 11 Research Scholars papers presented during the symposium cum workshop spread over 12 Technical Sessions. Invited speakers from overseas included Prof. Christopher M.A. Brett (Portugal), Prof. (Ms) A.M. Oliveira-Brett (Portugal), Prof. K. Vytras (Czech Republic), Prof. Hyacinthe Randriamahazaka

Group of participants on the event

(France), Prof. Chee-Seng Toh (Singapore) and Prof. Ritu Kataky (UK). The speakers from India included Prof. K. Girish Kumar (Kochi), Dr. Subir Kumar Ghosh (Mumbai), Prof. R.N. Goyal (Roorkee), Dr. Ida Tiwari (Varanasi), Dr. Sunil Bhand (Goa), Dr. Rajiv Prakash (Varanasi), Dr. G.S. Suresh (Bengaluru), Dr. N. Rajendran (Chennai), Prof. J.B. Fernandes (Goa), Dr. V. Dharuman (Karaikudi). Two short lectures were delivered by Mr. Saurav K. Guin (Mumbai) and Dr. Mohsin Ahmed Bhat (Srinagar). The scientific topics included advances in electrochemistry for biosensors, chemical sensors, room temperature ionic liquids, electrosynthesis of nano-particles, composite and modified electrodes, corrosion protection, voltammetry, coulometry, spectroelectrochemistry, preparation of inorganic fullerene, magnetic thin films, radionuclidic sources, molecular imprinted electrode, solid state electrochemistry, density function theory, electrochemistry of actinides, chiral electrochemistry, fuel cells, nanotubes, graphene and conducting polymer electrode materials etc. Besides,

there were tutorial lectures on DNA-electrochemical Biosensors, Electrochemical Impedance Spectroscopy, Carbon Paste Electrodes and Electrochemical Investigations of Self-assembled Monolayers and Lipid Bilayers.

During the valedictory function, some of the delegates were invited to give their impressions about the event. Merit certificates and cash awards were given to the authors of the best posters and best oral presentations. Prof. S.K. Aggarwal, Chairman, ISEAC-WS-2011, thanked all the delegates from India and Overseas, as well as sponsors, for their keen interest during the deliberations of the event. In particular, he thanked BRNS (DAE), CSIR and DRDO, International Society of Electrochemistry (ISE) and Bioelectrochemical Society (BES) for co-sponsoring the Symposium cum Workshop.

Fabrication and Quality Control of MOX Fuels (FQCMF-2012) : Report of a theme meeting

A theme meeting on " Fabrication and Quality Control of MOX Fuels" was held at AFFF Lecture Hall, BARC, Tarapur on March 16, 2012. The meeting was organized by the Advanced Fuel Fabrication Facility in association with Board of Research in Nuclear Sciences (BRNS), Department of Atomic Energy, Government of India. The meeting was inaugurated by Dr. S. Banerjee, Chairman, Atomic Energy Commission. Dr. Banerjee in his inaugural speech emphasized the need of nuclear energy in our country and the safety of our reactors. He stressed on the importance of fuel fabrication for the forthcoming fast reactor at Kalapakkam. It was followed by presidential address of Dr. R K Sinha, Director, BARC. He conveyed that AFFF has the mandate of fabricating the fuel for the first core and

he said that operation of fast reactor with indigenous fuel will be a landmark in Nuclear Power Programme. He also appreciated the safety norms that are being followed during the handling of radioactive materials. Dr. G J Prasad, Director, Nuclear Fuels Group welcomed all the guests and appreciated for the keen interest shown by different groups of DAE for participating in this theme meeting. Dr. Jose P Panakkal, Head, AFFF in his introductory remark mentioned that fabrication of forty thousand pins for PFBR is a challenging task and AFFF is determined to complete this task. In the past also, it has fabricated fuels for different types of reactors and all of them have been irradiated successfully. Md. Afzal, Plant Superintendent, AFFF was instrumental in comparing the inaugural session

Dr. Srikumar Banerjee, Chairman, AEC and Dr. R. K. Sinha, Director, BARC with other Senior officers of BARC at the innaugural event

and proposed a vote of thanks. Among the other dignitaries present on the dais was Shri S Basu, Chief Executive, Nuclear Recycle Board.

The meeting was divided in two sessions. The Session-I began with the key note address by Dr. Jose P Panakkal on MOX fuel programme in India. In his presentation, he covered the fabrication procedure followed for fabrication and quality control of MOX fuel, new techniques developed for fabrication, process, quality control and characterization of fuels.

The key note address was followed by invited talks. Dr. K L Ramakumar briefed about the chemical quality control measurements for MOX fuel. He explained to the participants how analytical chemistry is indispensable and plays an important role in the entire nuclear fuel cycle activities starting from ore refining, conversion, nuclear fuel fabrication, reactor operation, nuclear fuel reprocessing to waste management. Since India is fabricating fuels for various types of reactors, a number of analytical parameters need to be determined as a part of chemical quality control of nuclear materials. Chemical quality control provides a means to ensure that the quality of the fabricated fuel conforms to the chemical specifications for the fuel laid down by the fuel designer. His talk covered analytical methodology for chemical quality control measurements, criteria for selection of analytical techniques and statistical treatment required to express the analytical results.

The next talk was delivered by Shri Arun Kumar, Associate Director, NFG. His talk was on evolution of MOX fuel for thermal reactors. He explained that though plutonium is more suitable to fast reactors due to its neutronic characteristics, recycling of plutonium in thermal reactors is in use due to various factors like reduction in demand of natural uranium, increasing the design burn up of fuel and disposition of plutonium of military origin. Starting form explaining the use of MOX in thermal reactors world wide, he narrated the works carried out in Indian scenario. He conveyed to the audience that the MOX

fuel fabrication for thermal reactors has led to the development of various novel technology and techniques which has given a strong base for fabrication of $(U-Pu)O_2$ MOX fuel on industrial scale for our fast reactor programme.

The first session was chaired by Dr. A K Suri, Director, Materials Group.

The Second session started with the presentation of Dr. T Jayakumar, Dirctor, Metallurgy and Materials Group, IGCAR on performance evaluation of mixed carbide and mixed oxide fuels irradiated in FBTR. He told that systematic performance evaluation of the fuel through Post Irradiation Examination (PIE) at different burn ups has enabled understanding the behavior of plutonium rich carbide fuel and provided the confidence in increasing the burn up in stages to a maximum of 165 Gwd/t well beyond the initial burn up limit. He also explained how the beginning of life gap closure behavior was evaluated using an experimental PFBR MOX fuel pin having the fuel composition $(U_{0.71}Pu_{0.29})O_2$. The feedback from the PIE on the MOX fuel performance will be useful for the designers to arrive at the optimum fuel specifications.

Shri S. Anantraman, Head, PIED delivered a talk on the Post irradiation studies on Mixed oxide fuels. He briefed that Post irradiation examination is an integral part of any fuel development programme. His paper provided a brief review of results of the examination and explained the difference between the irradiation performance of urania - plutonia MOX fuels from that of thoria - plutonia MOX fuels.

Md. Afzal, Plant Superintendent, AFFF discussed the experience in the fabrication of MOX fuel. His presentation was detailed deliberation of glove box design, process equipment design and automation system for plutonium based fuel fabrication. He explained how the design of glove box, process equipment and the automation system should take into account the three constraints of the availability of space, occupancy and geometry of the fabrication

equipment, visibility and approachability in the glove box. Implementation of the interlinked design as a whole overcomes the constraints imposed by the glove box.

Shri G V S Hemanth Rao, DCE, Nuclear Fuel Complex presented the fabrication of fuel subassemblies for fast reactors. He informed that manufacturing capability of Indian industry was used effectively for precision components. Special purpose machines required for variety of assembly operation were developed indigenously. Fabrication operations were mastered including optimization of process parameters and quality control techniques. Welding operations typical to FBTR and PFBR component fabrication were developed in house successfully with the help of fixtures and tooling specifically developed for this purpose.

Shri D Mukherjee, Head, MES, QAD talked on quality surveillance of MOX fuels. Quality surveillance of nuclear fuels include all the technical and management aspects of fuel quality and safety during the entire manufacturing process. Well structured quality assurance programme is adopted and incorporated in the quality control plan made based on approved specification for a specific MOX fuel type used in a specific reactor (BWR, PHWR, PFBR).

The second session was chaired by Dr. G J Prasad, Director, Nuclear Fuels Group.
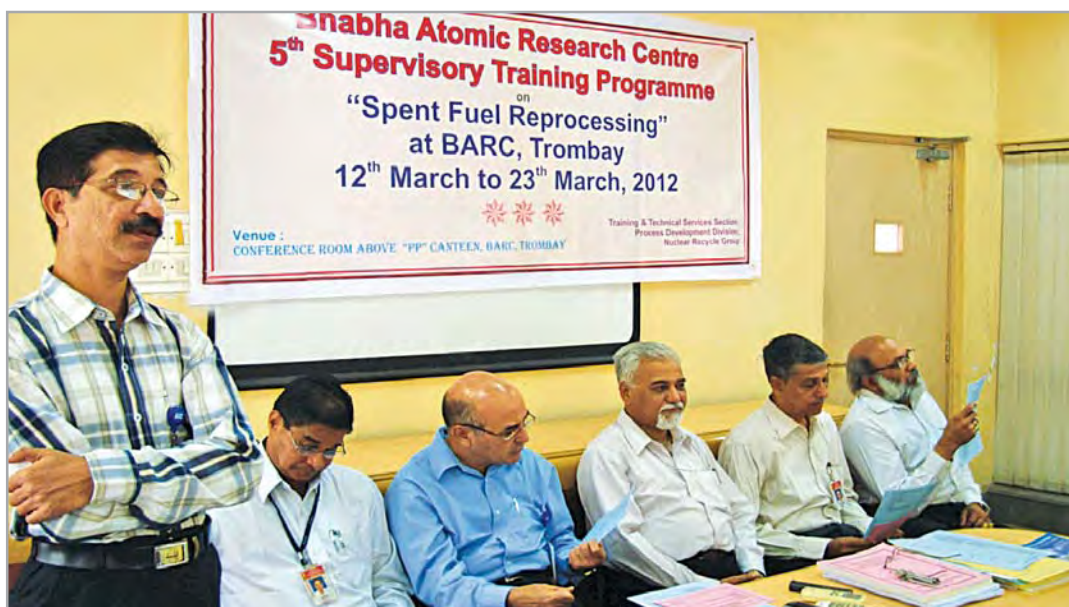
"Fifth Supervisory Training Programme on Spent Fuel Reprocessing": a report

The Fifth supervisory training programme on "Spent Fuel Reprocessing" was conducted at BARC, Trombay by the Nuclear Recycle Group during March 12th, 2012 to March 22nd, 2012.

This programme covered various aspects of nuclear fuel, fuel fabrication, generation of spent fuel reprocessing, associated auxiliary systems in reprocessing plants, emerging solvent/ technologies, thorium fuel reprocessing and projects related to reprocessing including integrated plant. Apart from these, the training programme also covered topics of safety such as health physics aspects, chemical safety, electrical safety, safety during material handling and handling of radiation emergencies, medical emergencies, etc.

The training programme was designed and organized by Shri R. G. Yeotikar, Officer-in-Charge, Training,

NRG and conducted and coordinated by Shri P. N. Patil, Shri Ved Ram Shakya and Shri P. Patange. Total 65 participants attended this supervisory training programme from reprocessing and waste management plants/facilities/projects from Trombay, Tarapur and Kalpakkam. Apart from these, the supervisors from other Divisions of BARC, Trombay, such as ROD, RCD, AFD, RMD, FCD, UED, etc. also attended this course. The training programme was carried out by way of classroom lectures, demonstrations and visits to various plant / facilities at Trombay such as Plutonium Plant, Waste Immobilization Plant, RSMS, ETP, AFD and Dhruva reactor. Faculty members, who are specialists in their fields with many years of experience, were invited from NRG and from AFD, ROD, IHSS, Hospital, Fire Station, etc., to deliver the lectures.

Inaugural Function of Fifth Supervisory Training Programme was held on 12th March 2012.
In the inaugural function, Mr. P. N. Patil, Coordinator of the training programme, welcomed the dignitaries and the participants present. Others on the dais (from left to right) are Mr. P. Janardan, Head, FRD; Mr. P. K. Wattal, Head, PSDD; Mr. R. G. Yeotikar, Office-in-Charge, Training, NRG; Mr. K.N.S. Nair, Head, TDD and Mr. P. M. Gandhi, CS,RF, PP.

BARC Scientists Honoured

Name of the Scientists	:	**A.D. Das and H.S. Misra** **Molecular Biology Division**
Title of the paper	:	A novel member of the beta-CASP family of nuclease is involved in the survivai of *Deinococcus radiodurans*
Award	:	AMI-Dr. Rana Memorial Best Poster Award presented to Shri A.D. Das
Presented at	:	during the 52nd Annual Conference of Association of Microbiologists of India (AMI) held at Punjab University, Chandigarh, from Nov.3-6, 2011

Name of the Scientists	:	**S. Mukhopadhyay, L.S. Danu, D.C. Biswas, P.N. Prashanth, A. Goswami, A. Chatterjee and R.K. Choudhury** **Nuclear Physics Division**
Title of the paper	:	"Yrast and near-yrast spectroscopy of neutron-rich fission fragments using thermal neutrons from reactor"
Award	:	First prize for Best Poster Presentation
Presented at	:	DAE Symposium on Nuclear Physics, held at Andhra university, Visakhapatnam, during December 26-30, 2011

Name of the Scientists	:	**P.C. Rout, T. Basak, D.R. Chakrabarty, V.M. Datar, Suresh Kumar, E.T. Mirgule, A. Mitra, S.P. Behera, G. Mishra and R. Kujur** **Nuclear Physics Division**
Title of the paper	:	Characterization of a liquid scintiliator detector using mono-energetic neutrons
Award	:	Second prize for Best Poster Presentation
Presented at	:	DAE Symposium on Nuclear Physics, held at Andhra university, Visakhapatnam, December 26-30, 2011

Name of the Scientists	:	**Y. S. Rajpurohit and H. S. Misra** **Molecular Biology Division**
Title of the paper	:	PprA phosphoryiation hy STPK of *Deinococcus radiodurans* changes its *in vitro* functions
Award	:	Best Poster Award presented to Y. S. Rajpurohit
Presented at	:	During 6th DAE-BRNS Life Science Symposiumm2011 (LSS-20l1) held at Bhabha Atomic Research Centre, Mumbai, from October 12-14, 2011

Name of the Scientists	:	**Rohit Shukla, Surender Kumar Sharma, Partha Bannerjee, Pankaj Deb, T. Prabaharan, Rashmita Das, Basanta Das, Biswajit Adhikary, Rishi Verma and Anurag Shyam** **Nuclear Physics Division**
Title of the paper	:	Microwave Emission from a AXIAL-Virtual Cathode Oscillation Driven by Compact Pulsed Power Source
Award	:	Best Poster Award and a Cash award of Rs. 5000/-
Presented at	:	International Symposium on Vacuum Science & Technology and its Application for Accelerators -2012 was held in VECC Kolkata during 15-17, February 2012

V. R. Chavan
Wooden Art Work